2017

Interaction Between Carbon Nanotubes and Metals (Al, Cu) and the Effects on Resultant Properties of the Hybrid Materials

Jingyin Jiang
University of Central Florida

ELECTRONIC STRUCTURE OF METAL (AL, CU) DOPED CARBON NANOTUBES AND THE RESULTANT CONDUCTION OF THE HYBRID MATERIALS

by

JINGYIN JIANG

B.S. Nankai University, 2012

A dissertation submitted in partial fulfillment of the requirements
for the degree of Doctor of Philosophy
in the Department of Materials Science and Engineering
in the College of Engineering and Computer Science
at the University of Central Florida
Orlando, Florida

Spring Term
2017

Major Professor: Quanfang Chen

ABSTRACT

Due to the exceptional strength, stiffness and excellent electrical and thermal properties, carbon nanotubes (CNTs) have been regarded as promising candidates for advanced nanoelectronics and multifunctional nanocomposites. In this dissertation, the interaction of CNTs with metals have been investigated and the resultant electrical conduction have been analyzed, aiming to develop innovative avenues to best utilize CNTs' potential. In order to do so, quantum mechanics calculations have been carried out to study that how to obtain greater electrical conduction by doping metals (Cu, Al) which tailor the electronic structure of three different types of metal-CNT interactions, : 1) encapsulation of atoms inside the CNTs, 2) adsorption of atoms onto CNT surface, and 3) substitutional doping. Models of different doping methods were built and optimized with Density Functional Theory (DFT). And in conjunction with non-equilibrium Green's function, the electronic structure and the conducting properties were then calculated.

Through this study, both metallic and semiconducting CNTs have been used. Metallic CNT (5, 5) encapsulated with copper chains have been first investigated with an emphasis on the electronic structure and the resultant conductance. The Density of States (DOS) have showed that the encapsulation of Cu effectively introduced more states around the fermi level. And due to the interaction between copper and CNTs, the conductance of the metallic CNTs-Cu system can be significantly increased.

In addition to copper, aluminum has been also introduced for the study. The electronic structure and transport properties of hybrid nanowires consisting of aluminum chains adsorbed on a single-wall semiconducting CNT (10, 0) have been calculated. The band structure and DOS of the hybrid nanowires have showed that the adsorption of Al can effectively reduce the band gap. And with more than 4 Al chains adsorbed, the CNT has transformed from semiconducting to conducting. The transmission eigenstates further indicated that both Al chains and the modified nanotube were responsible for the increased conduction in the hybrid nanowires. The resultant conductance of CNT (10, 0)/Al hybrid nanowire is about 40% greater than that of pure Cu nanowire with the same diameter.

In order to utilize the extraordinary conductance in CNT(10,0)/Al hybrid nanowire, it is also important to investigate the end-contact between the hybrid nanowire with Al electrodes. During this work the transmission spectrum at different bias voltage were calculated to study the I-V characteristics and the electrical contact resistances at the interfaces. The results have suggested that the electrical contact resistances between Al electrodes and the hybrid nanowire is significantly lower than that of Al-pure CNT contacts, although the actual contact resistance is directional dependent that the contact resistance is reduced to 20% of that Al-pure CNT along the longitudinal direction.

The possibility of substitutional doping of Cu and Al in both metallic and semiconducting CNTs were also investigated. The formation energies have showed that Al doping was more energy favorable than Cu doping in both cases. And by doping of Al or Cu, a metallic tube experienced a higher conductance and a semiconducting tube has transited to conducting.

In summary, different doping methods could modify the conducting property of nanotubes. Encapsulation of Cu in metallic CNT results in a significant conductance increment. Adsorption of Al transforms semiconducting CNT to conducting and reduces the contact resistance between the nanowire and Al electrode. Substitutional doping of Cu or Al transits semiconducting nanotube to conducting and enhance the conductance of metallic nanotube.

ACKNOWLEDGMENT

I would like to express my very great appreciation to my advisor Dr. Quanfang Chen, for his inappreciable guidance, valuable advice and support toward successful completion of my doctoral course. And I would also acknowledge Dr. Jiyu Fang, Dr. Lei Zhai, Dr. Yuanli Bai, and Dr. Sergey Stolbov for serving as my committee members. Besides, I thank my fellow lab mates for their stimulating discussion and friendship. In particular, I am grateful to Dr. Chengyu Yang for enlightening me the first glance of research.

In addition, I want to express my deep gratitude to my parents who brought me into this world with all the best and to my mother in law, who cares me with her heart and gives me a lot of help. And also many thanks to my best friends, Jingyi Wang and Ying Qin who warmed me with their companion.

Last but not least, I would like to thank my husband, whose love and wisdom has lightened my life. I would also like to acknowledge my son, Timothy Wang, who was born along with this dissertation.

TABLE OF CONTENTS

LIST OF FIGURES

LIST OF TABLES

LIST OF ACRONYMS/ABBREVIATIONS

CNT	Carbon Nanotube
DFT	Density Functional Theory
NEGF	Non-equilibrium Green's Functional Theory

CHAPTER 1 : INTRODUCTION

1.1 Carbon Nanotube Discovery

In 1991, multiwall carbon nanotube (MWCNT) was first discovered on the cathode of carbon arc during the DC arcing of graphite by Professor Iijima's group.[1] Two years later, in the same group, observation of single wall nanotubes (SWNT) was made in arc process in the presence of Fe or Co catalytic particles[2]. Afterwards researches on carbon nanotube fabrication were quite popular all around the world. In 1998, Ren et al[3] used Chemical Vapor Deposition (CVD) produced aligned MWCNT films in the presence of catalyst. Schlittler et al[4] successfully synthesis ordered single crystal of SWNT of micro sizes in 2001. With more advanced technology of fabrication, people started to explore the potential of carbon nanotube and found its excellent optical, mechanical and electronic properties of Single Wall Carbon Nanotube (SWCNT). It has drawn people's attention to put even more research effort on it. With better understanding on carbon nanotubes, broader applications including carbon nanotube transistor [5], solar cells[6], hydrogen storage[7] and interconnects[8] become reality nowadays.

1.2 Carbon Nanotube's Structure

Nano materials made of carbon can be divided into four classifications according to its dimension: zero dimensional structure (fullerenes, carbon onions), one dimensional structure (carbon nanotube), two dimensional structure (graphene), and three dimensional structure (nanocrystalline diamond). These configurations are schematically shown in Figure 1-1. A SWCNT can be considered as a graphene sheet rolled into a hollow cylinder in a particular direction.

Diameter of a SWCNT can be nanometers up to micrometers. And a SWCNT can be up to millimeters in length. Assume the rolling starts from a carbon atom in a Benzene ring. Set it as the original point and this Benzene ring is labeled as (0, 0). Use the coordinates $\overrightarrow{a_1}, \overrightarrow{a_2}$ as shown in Figure 1-2 thus each benzene ring can be labeled in the coordinates. When the graphene is rolled in a particular direction, a benzene ring (n, m) matches the benzene ring (0, 0) then we call the carbon nanotube formed CNT (n, m). The rolling angle θ is the angle between $\overrightarrow{a_1}$ and the line

formed by connecting (0, 0) with (n, m). Normally people use $\overrightarrow{C_h}$ to present the rolling direction as:

$$\overrightarrow{C_h} = \mathrm{n}\overrightarrow{a_1} + \mathrm{m}\overrightarrow{a_2} \quad (1\text{-}1)$$

When θ=0°, (Figure 1-3a), the carbon nanotube formed is zigzag CNT (shown as Figure 1-3(a)). When θ=30°, armchair CNT (shown as Figure 1-3(a)) is formed. Chiral CNT is formed when 0°<θ<30°. Figure 1-3(b) illustratively shows the configuration of the three types of SWCNT. And the different types of SWCNTs can also be defined by using n and m value.

-armchair CNTs (n=m) have C-C bonds perpendicular to tube axis.

-zigzag shaped CNTs (m=0) have C-C bonds parallel to tube axis

-chiral CNTs (n ≠ m) have the shape between armchair CNTs and zigzag CNTs.

The primitive vector $\vec{T}$ of one-dimensional lattice is defined as the shortest vector of the graphene lattice. Assume$\vec{T} = t_1\overrightarrow{a_1} + t_2\overrightarrow{a_2}$. Since the primitive vector is perpendicular to rolling direction, we have$\overrightarrow{C_h} * \vec{T} = 0$. So that it is easy to get

$$t_1 = \frac{2\mathrm{m} + \mathrm{n}}{\mathrm{N}_R}, t_2 = \frac{2\mathrm{n} + \mathrm{m}}{\mathrm{N}_{Rg}} \quad (1\text{-}2)$$

Where, $\mathrm{N_R}$ is the greatest common divisor of (2m+n) and (2n+m). Translational period *t* along the tube axis is defined as the smallest graphene lattice vector $\vec{T}$ perpendicular to$\overrightarrow{C_h}$. The length of translational vector *t* is given by

$$t = \frac{\sqrt{3}a\sqrt{n^2 + nm + m^2}}{N_R} \quad (1\text{-}3)$$

Thus the formed CNT has a height *t* and diameter *D*. The number of carbon atoms per unit cell N_c can be expressed as

$$N_c = \frac{4(n^2 + nm + m^2)}{N_R} \tag{1-4}$$

schematic view	entity
	Fullerene
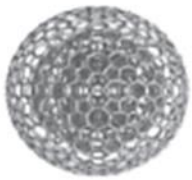	Carbon onions
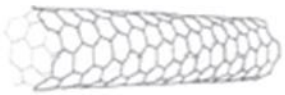	Single wall nanotubes (SWNT)
	Multiwall nanotubes (MWNT)
	SWNT ropes SWNT single crystals [51,58]
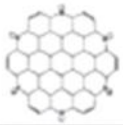	Single Graphene sheet
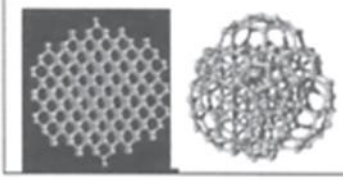	Diamond nanoparticles 'bucky' diamond (right)

Figure 1-1 Different Carbon Nano Structure Family

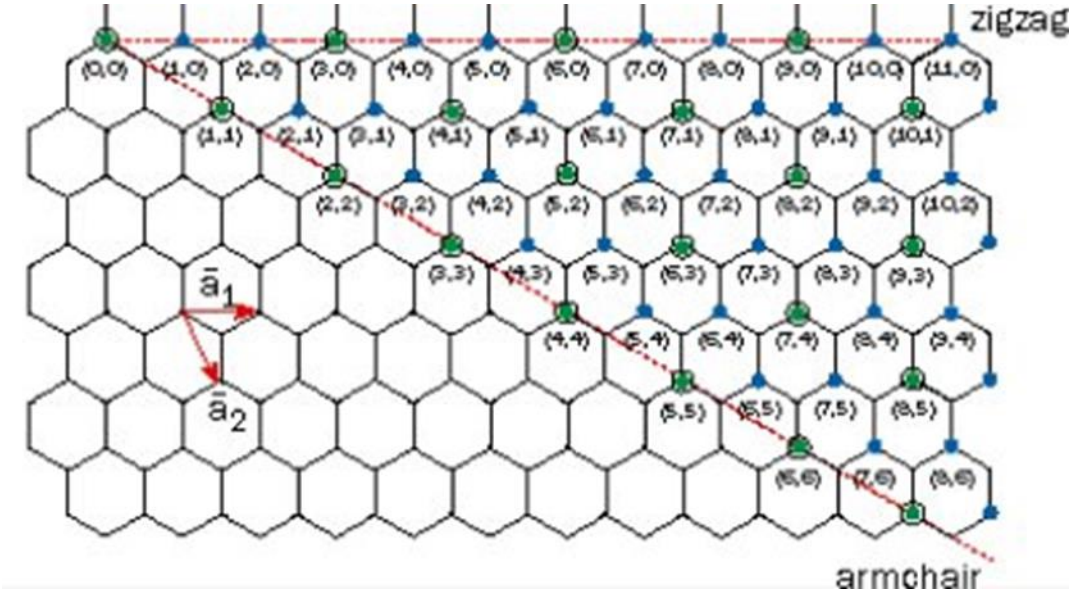

Figure 1-2 Schematic Drawing of Graphene[9]

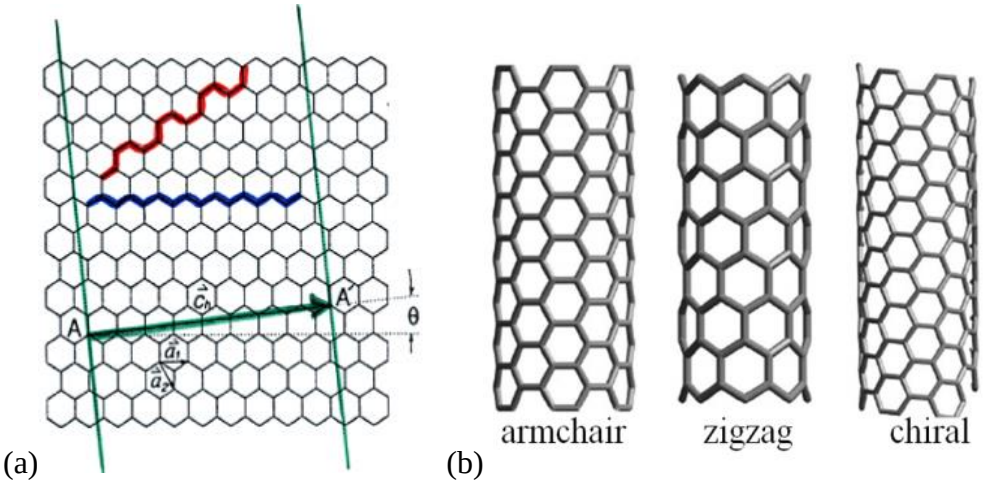

(a) (b)

Figure 1-3 (a) Schematic Drawing of How Graphene Roll up into Carbon Nanotube[9]; (b) Different Carbon Nanotubes

1.3 Properties of Carbon Nanotube

1.3.1 Band Structure of Graphene

The band structure of graphene is essential for understanding the conduction of a SWCNT. A carbon atom has four valence electron in atomic orbitals of 2s, 2px, 2py, and 2pz. Graphene can be considered as array of carbon atoms arranged in a hexagonal lattice shown as Figure 1-4. Each atom will form sp2 hybridization molecular orbitals (here we call it σ hybridization orbitals) with its 2s, 2px, 2py orbitals and covalently bonds to its neighbor carbon atoms. The fourth orbital pz, for symmetry reasons, does not couple with σ hybridization orbitals but hybridizes with all the other pz orbitals to form a delocalized π orbitals. The schematically σ and π orbitals of an individual carbon atom in graphene are shown in left side of Figure 1-4[10]. On the right side of Figure 1-4 presents the first Brillouin zone of graphene. In Figure 1-5 a large energy gap between the bonding (occupied) σ and antibonding (unoccupied) σ* can be observed. Both σ and σ* are far away from the Fermi level. However, bonding π and antibonding π* bands do cross the Fermi level at K points[11]. Generally speaking, the electrons (holes) near the Fermi level attribute to electrical transport properties, since they have easy access to the unoccupied (occupied) states. Thus the discussion of π and π* bands are crucial here. The surface and contour plots of the energy dispersion are also shown in Figure 1-6 (a) and (b), respectively. The main feature of the Fermi surface of graphene is therefore reduced to the six K points at the corner of the Brillouin zone, where the conduction and valence bands meet and thus the band gap is zero. At six K points, the conic energy dispersion as shown in Figure 1-6(a) can be found. The density of states (DOS) in graphene can be derived from the energy dispersion relation and it is found to be zero at the Fermi level. Consider this with the zero bandgap, graphene is also called a zero bandgap semiconductor.

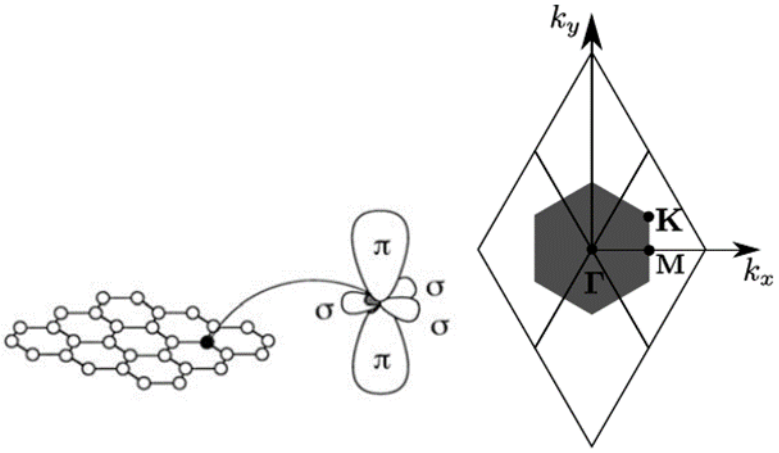

Figure 1-4 Left: The carbon valence orbitals: Left: The carbon valence orbitals: in planar σ and perpendicular π orbitals. Right: reciprocal or lattice of graphene is real space Bravais lattice of graphene, rotated for π/2. The first Brillouin zone is shaded and the three important points are noted: center Γ, corner K and middle of the edge M point.[10]

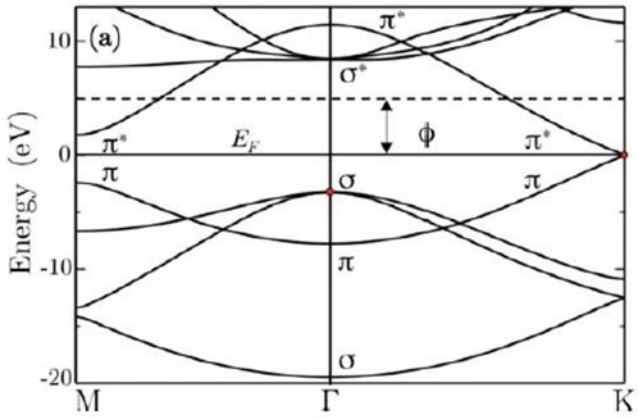

Figure 1-5 Electronic Band Structure of Graphene.[11]

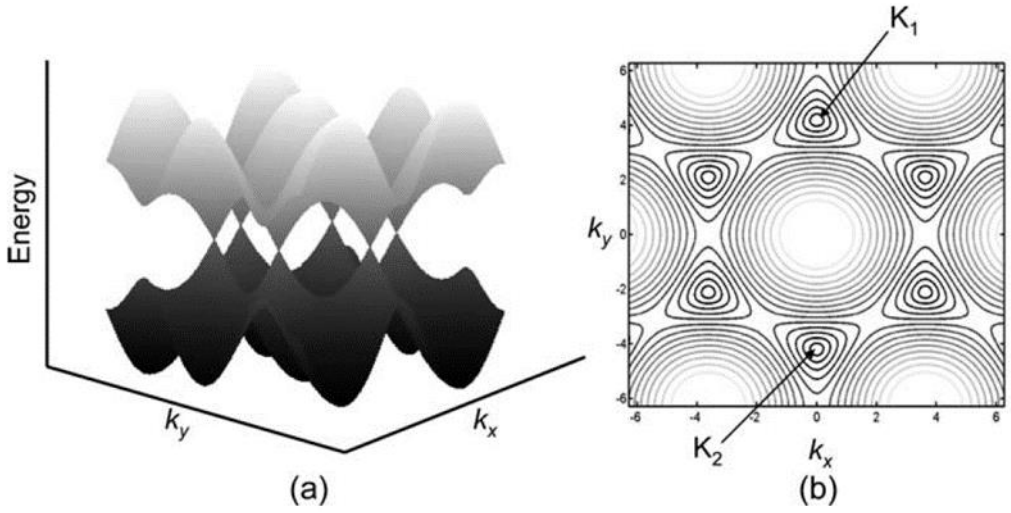

Figure 1-6 (a) Surface plot and (b) contour plot of the energy dispersion in Graphene.

1.3.2 Band Structure of Single Wall Carbon Nanotube from Graphene

Applying the zone-folding approximation, the band structure of SWCNTs can be constructed from that of graphene by imposing the periodic boundary condition. Consider a SWCNT as an infinitely long cylinder, there are two wave vectors: $\overrightarrow{k_{\parallel}}$ which is parallel to the SWCNT axis, and $\overrightarrow{k_{\perp}}$ which is along the circumference of a SWCNT. According to the periodic boundary condition, the wave factor $\overrightarrow{k_{\perp}}$ should satisfy that

$$\overrightarrow{k_{\perp}} * \overrightarrow{C_h} = \pi d k_{\perp} = 2\pi m \tag{1-5}$$

Where *d* is the diameter of a SWCNT and *m* is an integer. This leads to quantized values of allowed $k_{\perp}$ for SWCNTs. From Figure 1-7, the 1D band structure of SWCNTs can be obtained by cutting the energy dispersion of 2D graphene with the allowed $k_{\perp}$ values. Each cross-sectional cutting gives a 1D subband. There is no bandgap when the allowed $k_{\perp}$ states pass through the K points as in Figure 1-7(b). The energy dispersion shows two linear bands crossing at the Fermi level. However, if the allowed $k_{\perp}$ states miss the K points as in Figure 1-7(c), the two parabolic 1D bands will have an energy bandgap. Usually some degeneracy exists and the number of different energy band is small. Examples of armchair CNT (5, 5), zigzag CNT (9, 0), and zigzag CNT (10, 0) are presented in Figure 1-8. The first two are metallic at finite temperature since they have zero bandgap and their valence and conduction bands cross at k=2π/3a (armchair) and k=0 (zigzag (9, 0)). The third zigzag (10, 0) has an energy bandgap (~1eV) and thus is referred to as semiconducting. To find the electronic properties of different CNTs, the rule can be applied as following: Assume n-m=3q+p. if p=0, then this type of CNT will be metallic with linear sub bands crossing at the K points. Otherwise, the CNT will be semiconducting with a bandgap and$\Delta E_g \sim 1/d$, where *d* is the diameter of the CNT.

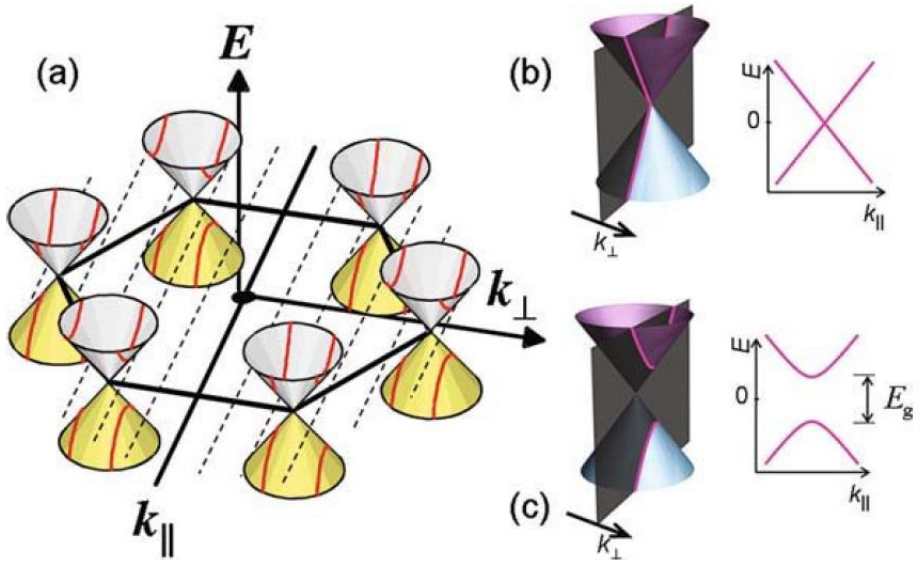

Figure 1-7 (a) A first Brillouin zone of graphene with conic energy dispersions at six K points. The allowed k states in a SWCNT are presented by dashed lines. The band structure of a SWCNT is obtained by cross-sections as indicated (b) a metallic SWCNT and (c) a semiconducting SWCNT.[12]

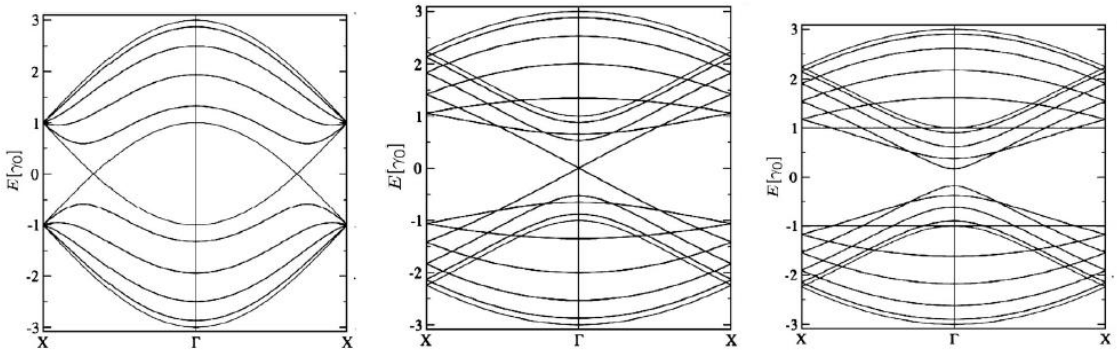

Figure 1-8 Energy Bands for Armchair (5, 5), Zig-zag (10, 0) tube, obtained by the zone folding approximation.[11]

However, in the zone-folding approximation it is assumed that π orbitals are still orthogonal to σ orbitals in the graphene plane. This assumption is actually not valid for SWCNTs due to the curvature which mixes π and σ orbitals. The hybridization between π and σ orbitals occurs in

SWCNTs, and the degree of the hybridization becomes larger as the diameter gets smaller. A small bandgap opens up in metallic SWCNTs with the consideration of $\pi - \sigma$ hybridization effect[13, 14], except in the armchair nanotubes due to the symmetry.

1.4 Electrical Transport in Single-Wall Carbon Nanotubes

A conductor is sandwiched between two contacts which is shown as Figure 1-9(a). The left and right regions consist of metals and ballistic conductor with length *L* and width *w* consist the middle region. If the device is a small nanometer length scale one, its transport property of electrons through the junction, i.e. current-voltage characteristic, needs to be considered as quantum effects. Dispersion relations for different transverse modes (or sub bands) in the narrow conductor is shown as Figure 1-9(b). There are reflections for higher-order transverse modes when electrons enter from a wide channel to a narrow channel. However, the reflection probability is negligible when electrons enter from a narrow channel to a wide channel, unless the mode is too close to cut-off. So for a reflection less contacts (Figure 1-10), the quasi-Fermi level for the +k states is μ_1 while that for the –k states is μ_2.

Consider the current carried by a single transverse mode and the discrete *k* states (Fourier mode) can be expressed as

$$k_N = \frac{2\pi}{\mathrm{L}} N \tag{1-6}$$

$$I^+ = e \cdot \frac{1}{L} \cdot \sum_k v f^+(E) \tag{1-7}$$

F-D distribution function

velocity $\frac{1}{\hbar}\frac{dE}{dk}$

summation over all *k*-states below μ_1

electron density (one electron per channel length *L*)

⇦ exclusion principle!

$$I^{+} = \frac{2\mathrm{e}}{\mathrm{h}} \int_{\epsilon_1}^{\infty} f^{+}(E) dE$$

(1-8)

If an external bias voltage is small and the number of transverse modes *M* above cur-off is constant over a small energy difference $\mu_1 < E < \mu_2$, then the net current is

$$\mathrm{I} = \frac{2e}{h} M\mu_1 - \frac{2e}{h} M\mu_2 = \frac{2e^2}{h} M\mathrm{V}$$

(1-9)

Where,

$$V = \frac{\mu_1 - \mu_2}{e} = \text{external bias voltage}$$

(1-10)

Considering the ballistic conductor in the central region has no scattering so the transmission probability equal to 1. Conductance G can be expressed as

$$G = \mathrm{G}_0 * M = \frac{2e^2}{h} M$$

(1-11)

And the resistance 1/G must be a contact resistance which comes with the dimensionality change on the contacts. If the conductor is not ballistic, the Landauer formula can be written as

$$G = \frac{2e^2}{h} MT$$

(1-12)

Where, T stands for transmission coefficient which gives the probability of electron transmission.

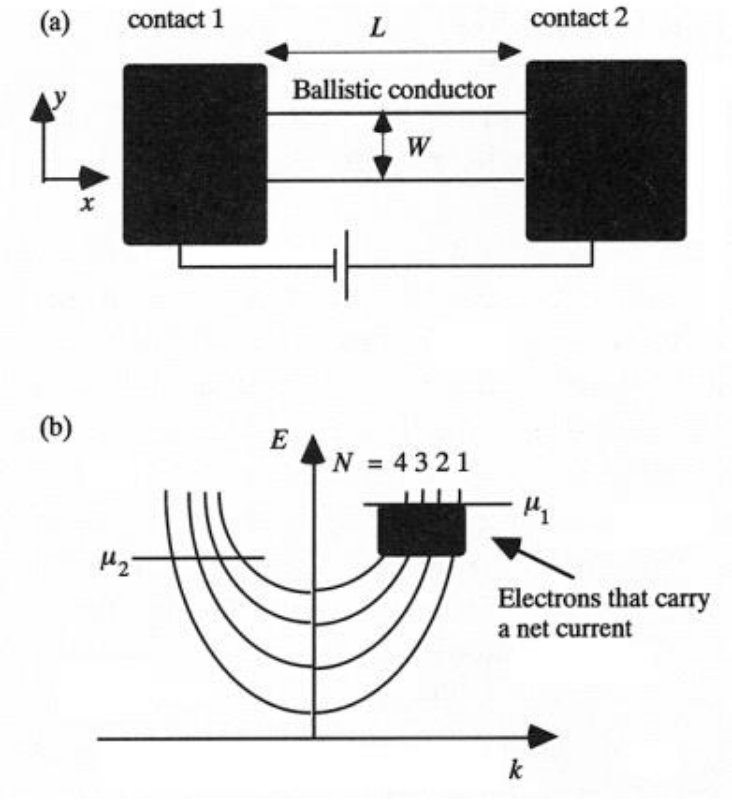

Figure 1-9 (a) A conductor is sandwiched between two contacts across which an external bias is applied. (b) Dispersion relations for the different transverse models in the narrow conductor.[15]

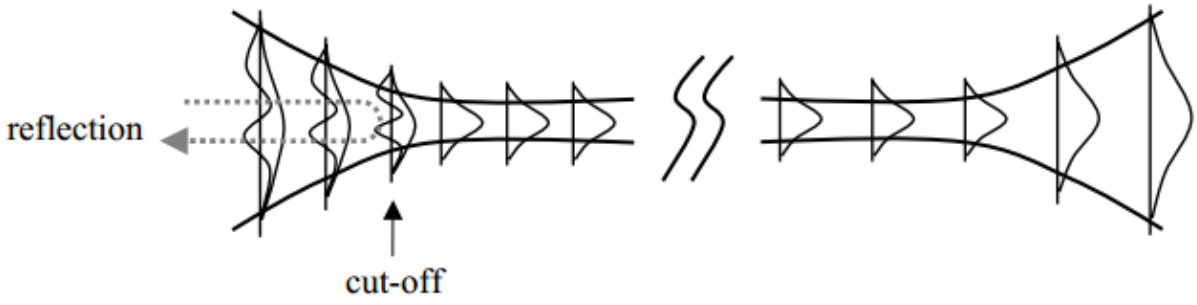

Figure 1-10 Reflection less contact

CHAPTER 2 : DENSITY FUNCTIONAL THEORY AND QUANTUMWISE

2.1 Density Functional Theory

Density functional Theory (DFT) is a variational method which computes the electronic structure of matters most successful upon now. DFT made it possible by the existence of two ingeniously theorems put forward and proved by Hohenberg and Kohn in 1964.

2.1.1 The first Hohenberg-Kohn Theorem

In 1964, Hohenberg and Kohn proved for any system of interaction particles in an external potential V(r), the corresponding ground-state electronic density n(r) is uniquely determined[16]. In another word, the argument that the energy is a function of charge density in Thomas-Fermi approach got confirmed and developed. based on the ground state electronic density, we can obtain the ground state wave function and other information easily.

2.1.2 The second Hohenberg-Kohn Theorem

The second Hohenberg-Kohn theorem states that a universal functional for the energy E[**n**] can be defined in terms of the density and the exact ground state is the global minimum value of this functional[16]. Variational Principle is applied here and it can be expressed as following:

$$E_v[\boldsymbol{n}] = F[\boldsymbol{n}] + \int n(\boldsymbol{r})V(\boldsymbol{r})\,d\boldsymbol{r} = < \Psi_{[n]} | \left(\hat{F} + \hat{V}\right) | \Psi_{[n]} > \tag{2-1}$$

$$E_v[\boldsymbol{n}] \geq E_0 \tag{2-2}$$

$$F[\boldsymbol{n}] = T_s[\boldsymbol{n}] + E_H[\boldsymbol{n}] + E_{xc}[\boldsymbol{n}] \tag{2-3}$$

$$E_H[\boldsymbol{n}] = \frac{1}{2}\iint \frac{n(\boldsymbol{r})n(\boldsymbol{r}')}{|\boldsymbol{r} - \boldsymbol{r}'|} d\boldsymbol{r}d\boldsymbol{r}' \tag{2-4}$$

2.1.3 Self-Consistent Kohn-Sham Equation

Finally, several well-known goodness-of-fit measures have been used to assess the recalibrated HSM algorithms as a whole, and the results are consistent as the results mentioned in the split investigation of HSM base model and CMFs. With these facts the authors concluded that the HSM is not suitable to transferable to Italy roads and Europe should orient towards developing local SPFs/CMFs.

Kohn and Sham system is based on Thomas-Fermi theory where every electron is regarded as moving in an effective single particle potential such that their ground-state charge density is identical to the charge density of the interacting system.

For a system with non-interacting electrons, the electrons are moving in an effective potential $V_s(\mathbf{r_i})$, and the Hamiltonian can be written as

$$\hat{H} = -\frac{1}{2}\sum_{i}^{N} {\nabla_i}^2 + \sum_{i}^{N} V_s(\boldsymbol{r_i}) \tag{2-5}$$

And the kinetic energy can be expressed as

$$T_s = -\frac{1}{2}\sum_{i}^{N} < \varphi_i|\nabla^2|\varphi_i > \tag{2-6}$$

Since this Hamilton operator does not contain any electron-electron interactions, it indeed describes a non-interacting system. For each specific orbital, we have

$$\left(-\frac{1}{2}\nabla^2 + V_s(\boldsymbol{r})\right)\varphi_i(\boldsymbol{r}) = \varepsilon_i\varphi_i(\boldsymbol{r}) \tag{2-7}$$

$$n(\boldsymbol{r}) = \sum_{i=1}^{N} |\varphi_i(\boldsymbol{r})|^2 \tag{2-8}$$

$$E = \sum_i \epsilon_i$$

(2-9)

Here, we can separate $V_s(\boldsymbol{r})$ as $V_s(\boldsymbol{r}) = v_H(\boldsymbol{r}) + v_{xc}(\boldsymbol{r}) + v_{ext}(\boldsymbol{r})$

(2-10)

Where,

$$v_H(\boldsymbol{r}) = \int \frac{n(\boldsymbol{r}')}{|\boldsymbol{r} - \boldsymbol{r}'|} d\boldsymbol{r}'$$

(2-11)

$$v_{xc}(\boldsymbol{r}) = \frac{\delta E_{xc}}{\delta n(\boldsymbol{r})}$$

(2-12)

The exact kinetic energy of the non-interacting reference system as that of the real interacting one is used here. The non-interacting kinetic energy is not equal to the true kinetic energy of the interacting system, so the exchange-correlation energy E_{xc} is added here as the residual part. Actually E_{xc} contains everything that is unknown[16]. It is the integral of the exchange correlation potential $v_{xc}(\boldsymbol{r})$ with respect to $n(\boldsymbol{r})$. Hence, the choice of good E_{xc} approximation is crucial to get an accurate results.

2.2 Non-equilibrium Green's Function Method

When people are dealing with ballistic conduction at nanoscale, non-equilibrium Green's function (NEGF) method is applied here. It is mainly used to calculate current and charge density of devices under bias voltages[17].

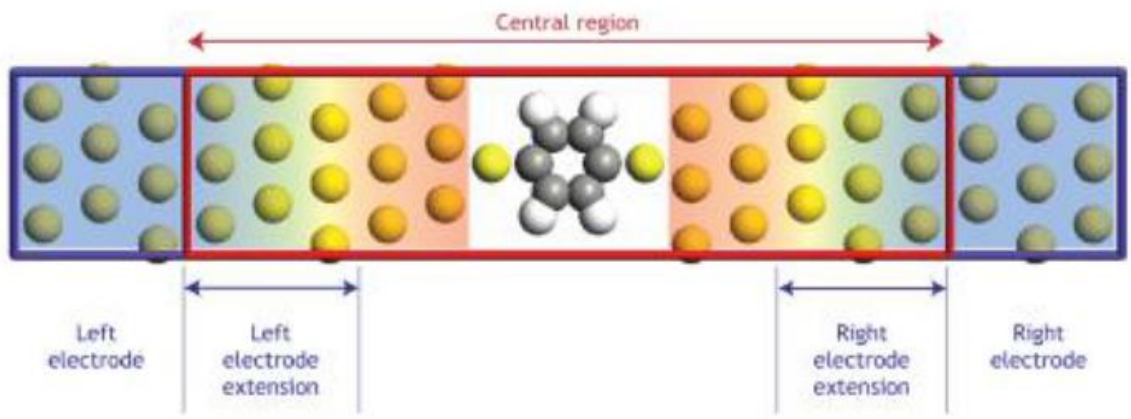

Figure 2-1 A Typical device system in QuantumWise[18]

A typical device system is shown as Figure 2-1. The device simply consists of three parts: left contacts, central part and right contacts. Usually periodic boundary conditions are applied in the left and right contacts, so that a conventional electronic structure calculation will give rich information of the device. The electrons in the central part are in non-equilibrium distribution, and Green's function can be expressed as[18]

$$G = [EI - H - \sum_L - \sum_R]^{-1} \tag{2-13}$$

Eq.2-13 is the definition for Green's function for such a device of a conductor coupled with two electrodes. $\sum_L \; and \; \sum_R$ are called self-energies of the left and right electrode.

In NEGF the electron density is given in terms of the charge density matrix. The left density matrix contributes ρ^L and

$$\rho^L = \frac{1}{2\pi}\int_{E=-\infty}^{\infty} f(E,\mu_1) G_d \, \Gamma_{\,L} \, {G_d}^{+} dE \tag{2-14}$$

Where G_d is the retarded Green's function for the device and $\Gamma_{\,L}$ is the broadening function of the left electrode.

$$\Gamma_{\,L} = \tau_{\,L} a_L \, \tau_{\,L}^{\,+} = i(\sum_L - \sum_L{}^{+})$$

(2-15)

Considering the similar condition for right electrode, the total charge density is the sum over all contacts[17]:

$$\rho = \frac{2(for\ spin)}{2}\int_{E=-\infty}^{\infty} dE \sum_i f(E,\mu_i) G_d \Gamma_i G_d{}^+$$

(2-16)

If the transmission is defined as the trace of the matrix quantity, the current given by the Landauer formula is like following [19]:

$$\bar{T}(E) = Trace\left[\Gamma_1 G \Gamma_2 G^+\right]$$

(2-17)

$$I = \frac{q}{h}\int_{-\infty}^{+\infty} dE\, \bar{T}(E)\left[f_1(E) - f_2(E)\right]$$
$$= \frac{q}{h}\int_{-\infty}^{+\infty} dE\left[f_1(E) - f_2(E)\right] Trace\left[\Gamma_1 G \Gamma_2 G^+\right]$$

(2-18)

2.3 QuantumWise

QuantumWise offers Atomistic Toolkit which is a general-purpose atomic-scale modeling platform that combines a wide range of methods and models which can be used to study electronic structure and transport problems. It contains LCAO-based DFT method, plane-wave DFT method, semi-empirical tight binding method and classical potentials. Here we use its DFT method to do computational analysis. DFT theory transforms the many-body Schrodinger equation into a one-electron equation. Since each electron in a system is non-interacting moving in an effective potential, the potential need to be determined self-consistently. The flow chart in Figure 2-2 describes the self-consistent loop in DFT method.

The key parameter in the self-consistent loop is the density matrix. For open systems, the density matrix can be obtained by NEGF method. For closed or periodic systems, it is calculated using diagonalizing the Kohn-Sham Hailtonian.

It can also be presented by the following equations[20]:

$$\widehat{H_{lel}} = -\frac{\hbar}{2m}\nabla^2 + V^{eff}[n](r) \tag{2-19}$$

$$\widehat{H_{lel}}\,\Psi_{\alpha}(r) = \varepsilon_{\alpha}\,\Psi_{\alpha}(r) \tag{2-20}$$

$$n(r) = \sum_{\varepsilon_{\alpha}<\mu} |\Psi_{\alpha}(r)|^2 \tag{2-21}$$

The Density Matrix defines the electron density, and the electron density sets up an effective potential. From the effective potential, one can obtain the Kohn-Sham Hamiltonian. From the Hamiltonian one can determine the one-electron eigenstates by solving the one-electron Schrodinger equation. By summing all occupied one-electron eigenstates, the electron density is determined.

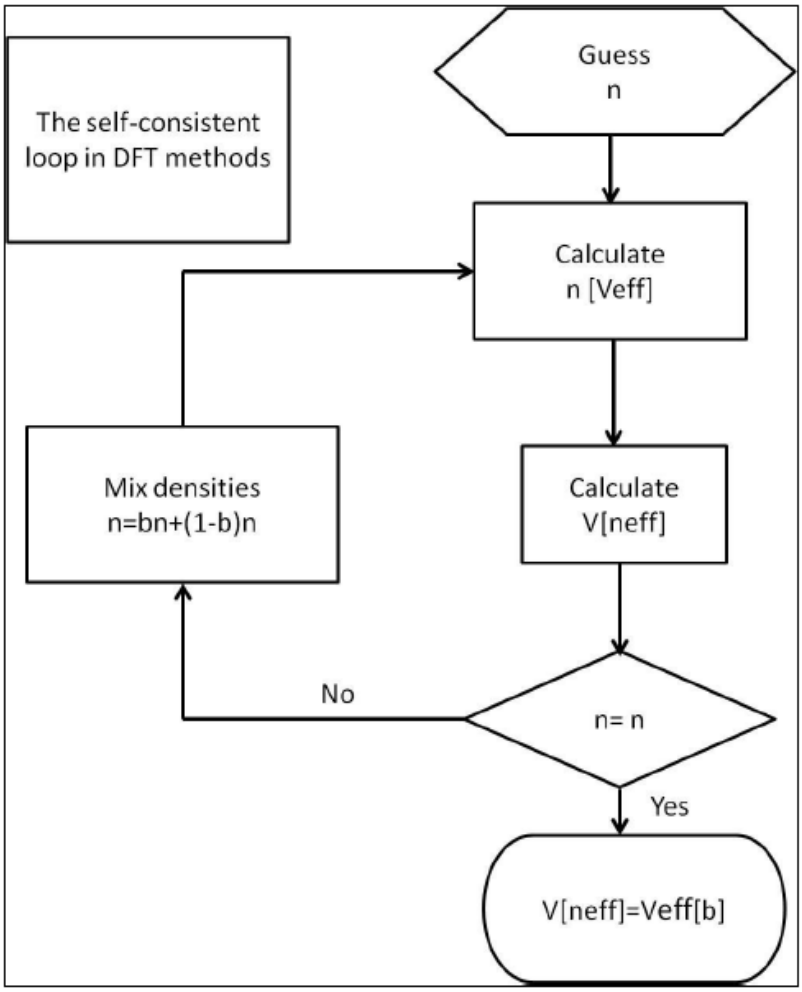

Figure 2-2 Flowchart for Density Functional Theory with self-consistent loop calculations.[20]

CHAPTER 3 : ELECTRONIC STRUCTURE OF COPPER DECORATED CARON NANOTUBE

3.1 Introduction

Single wall carbon nanotube (SWCNT) is a promising nanomaterial for the development of nanodevices, due to its extraordinary mechanical and electronic properties. The applications include nanotube-field effect transistor [21-25], solar cells [26, 27], hydrogen storage [7, 28, 29] and interconnects [30, 31]. However, current methods of nanotube synthesis produce a wide range of nanotube chirality, which will highly affect the product quality. Therefore, for practical application it requires the tailor able electronic properties on CNTs.

Modification of CNT's electronic properties by forming metal-CNT hybrid system was successfully fabricated that a continuous Titanium chain on carbon nanotube and the change on CNT's electronic structure has been reported [32]. It has also been pointed that the incorporation of a metal chain modifies the electronic structure of carbon nanotube via the charge transfer and the orbital hybridization [32-34]. Recently copper is used to decorate CNT into a novel one dimensional nanocomposite which combines the excellent properties of both CNT and metallic nanowire [35]. It is also reported that Copper/CNT hybrid system could improve the conductivity of CNT and even change the semiconducting CNTs to metallic ones [36]. However, no report can be identified about how the copper will influence the electronic properties of metallic CNTs. In this paper, authors have presented the influence of the interaction between copper chains and on metallic CNT's electronic properties.

3.2 Theoretical Approach

The model for this study is shown in Figure 3-1. On the left side, (a), (b),(c) and (d) show the unit cells for the different models of CNT (5, 5) encapsulating different number of copper chains (1, 2, 4, 5 chains, respectively). Each unit cell contains two copper atoms per copper chain. The configurations were all fully optimized using the QuantumWise/ (ATK13.8.1) package. All the calculations were performed in the framework of the density functional theory with fully self-consistent calculations in solving the norm-conserving Kohn-Sham (KS) equations [37]. In the

geometry optimization process the local density approximation (LDA) [38] with the Perdew-Zunger (PZ) exchange-correlation functional [39] was used. The right side of Figure 3-1 gives the side view of the atomic structure of different models (a) (b) (c) and (d) and the result of C_{160} (4 unit cells) is reported.

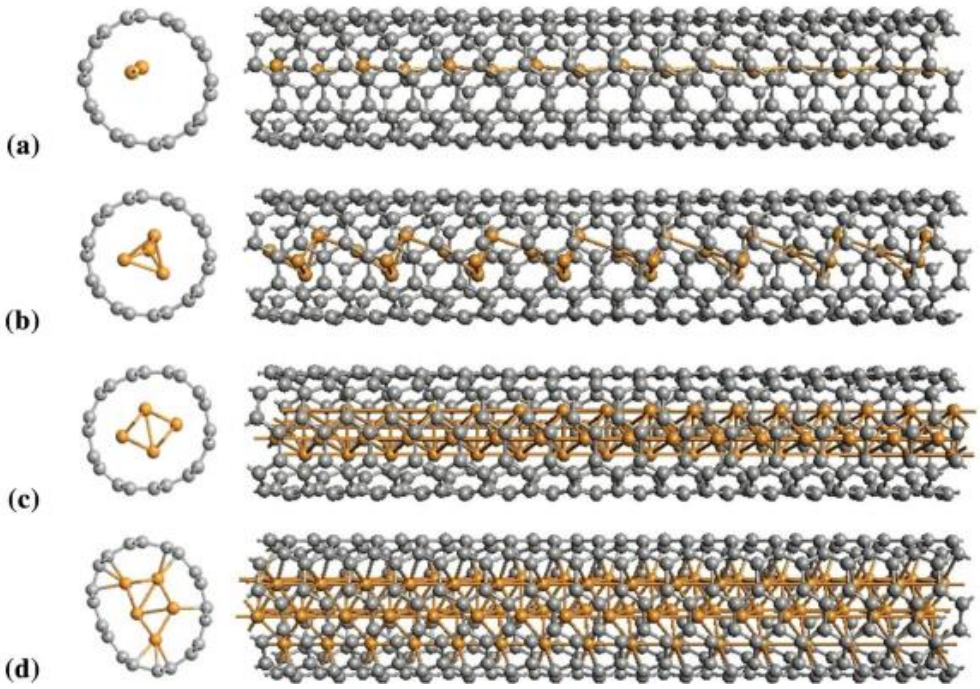

Figure 3-1 Configuration of CNT (5, 5)-Cu system with (a) one Cu chain; (b) two Cu chains; (c) four Cu chains; and (d) five Cu chains encapsulated.

For the relaxed geometries the electronic structure and the transport properties are calculated with the generalized gradient approximation (GGA) with the Perdew-Burke-Ernzerhof (PBE) exchange-correlation functional. $1*10^{-5}$ was used as the convergence criterion of total energy tolerance. Figure 3-1 shows the two probe models system constructed with CNT (5, 5) and 1, 2, 4, 5 copper chains encapsulated.

3.3 Results and Discussion

In Figure 3-1, a single copper chain sitting inside CNT (5, 5) is zigzag shaped along the z direction. It is observed from Figure 3-1 that CNT (5, 5) deforms to different extent with different number of copper chains encapsulated. It looks that the more copper chains were encapsulated the more deformation on CNT will cause. For the case of 5 copper chains the CNT becomes very asymmetric elliptical.

3.3.1 Binding Energy

The binding energy can E_b of copper encapsulation in CNT (5, 5) was computed by using the following equation:

$$E_b = E(CNT - Cu) - E(CNT) - E(Cu) \tag{3-1}$$

Where, E (CNT-Cu) represents the total energy of the CNT (5, 5)-Cu system, E (CNT) and E (Cu) represent the total energies of the isolated systems.

The binding energy of a single Cu atom encapsulated CNT (5, 5) is 1.18eV/atom. Compared to the low binding energy of Al/ Au on CNT (5, 5) (<0.5eV) [14], it indicates the interaction other than physisorption may exist between copper and CNT. Such higher binding energy may be favorable for the nucleation of copper atoms to form continuous wires in experiment.

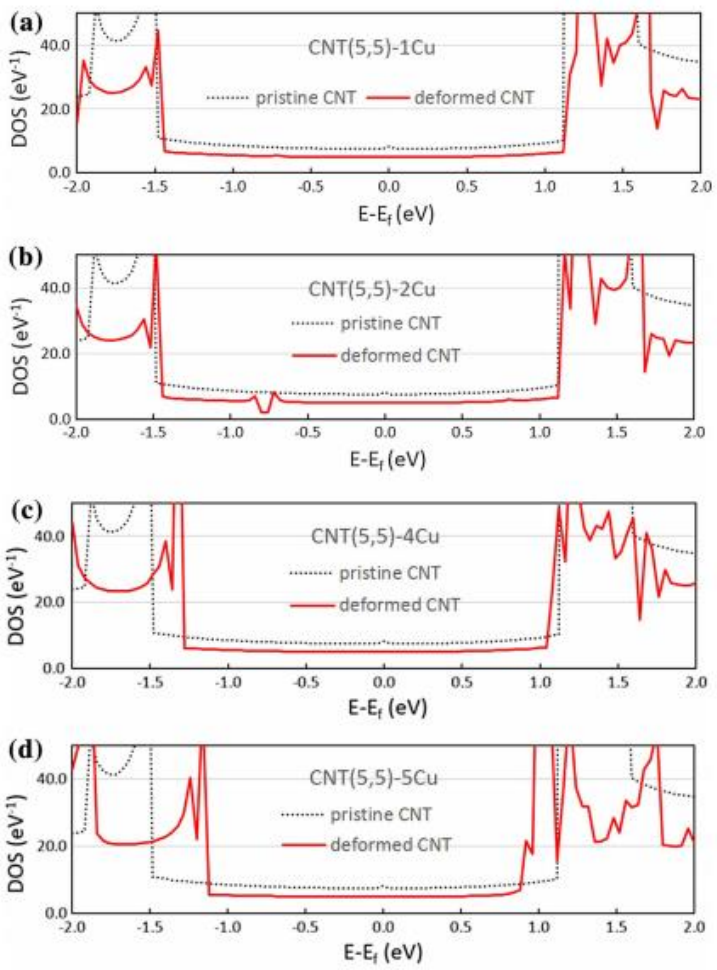

Figure 3-2 Density of States for CNT (5, 5) part of the CNT (5, 5)-Cu system with (a) one Cu chain; (b) two Cu chains; (c) four Cu chains; and (d) five Cu chains encapsulated.

3.3.2 Density of States (DOS)

The density of states (DOS) of the deformed CNT taken out from the Cu-CNT (5, 5) system encapsulated with 1, 2, 4, 5 chains are shown in Figure 3-2 (a), (b), (c) and (d) respectively. For a single copper chain encapsulated CNT, the DOS is 4.92eV at the Fermi lever, that is about 2.52 eV lower than that of the pristine CNT (8.27 eV), but the distribution of DOS stay almost the same as the pristine CNT that the DOS of the Cu encapsulated CNT shifts parallel down in contrast to the pristine CNT which indicates that the deformation of CNT may lower the DOS of CNT. From Figure 3-2(b) to (d), DOS of deformed CNT at Fermi level doesn't change much. However, the gap between peaks reduces to 2.32 eV with 4 copper chains encapsulated in CNT. And it shrinks

to 2.00 eV in CNT (5, 5)-5Cu hybrid system. It is believed that the deformation of CNT results the gap closer. To understand the CNT-Cu system, further analysis of DOS of the whole system is provided in Figure 3-3.

The density of states of Copper chains, the CNT (5, 5) and the coupled Cu/CNT systems are presented in Figure 3-3. In each diagram, the black line denotes the DOS of CNT (5, 5)-Cu chain system, the blue and red lines indicate the DOS of Cu chain and CNT part respectively. Figure 3-3(a) shows that a single copper chain has a large amount of states below Fermi level. For the CNT (5, 5)-1Cu system, significant amount of states are created below the Fermi level as well. This should be caused by the interaction of copper atoms and the CNT. With 2 copper chains encapsulated, it shows a larger amount of density of states at Fermi level in Figure 3-3(b), which is in consistence with the small peak of DOS of copper chains around Fermi level. For CNT (5, 5)-4Cu system in Figure 3-3(c), at the Fermi level the DOS of the system increases dramatically, though there are not many states for the copper part in the system.

The states are the product of interaction between the CNT and copper chains. The large deformation of CNT should be responsible for the interaction between the CNT and copper chains. Figure 3-3(d) presents the more evenly distributed high DOS around Fermi level for CNT-5Cu hybrid system. By comparison the average DOS of 5 Cu chains encapsulated system is larger than that of CNT-4Cu hybrid system at the Fermi level. These results indicate that the interaction between the carbon nanotube and the copper chains modifies each other's electronic structure.

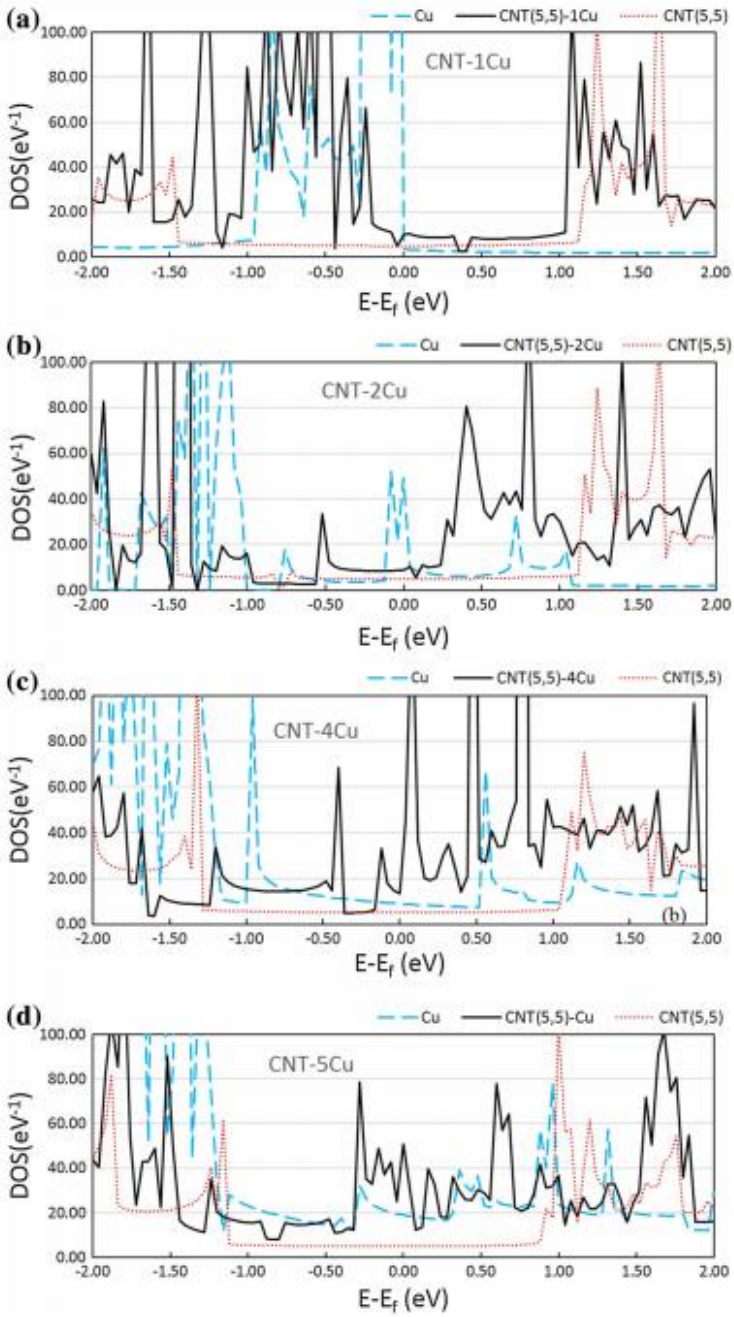

Figure 3-3 Density of States of CNT (5, 5)-Cu system with (a) one Cu chain; (b) two Cu chains; (c) four Cu chains; and (d) five Cu chains adsorbed.

3.3.3 Local Density of States (LDOS)

The isosurface of local density of states (LDOS) at Fermi level for CNT (5, 5) – Cu chains hybrid system is shown in Figure 3-4. For single copper chain encapsulation system, most of the states are located on the copper chain, which is in agreement with the DOS graph shown in Figure 3-3(a). Here we can further understand that the most density of states of CNT (5, 5) -1 Cu system is offered by the copper atoms. When two copper chains are introduced into the hybrid system, the density of states tends to be uniformly located both on the copper chains and the carbon nanotube. The density of states increases largely and uniformly with 4 copper chains encapsulated. However, due to the asymmetrically distribution of copper atoms and the carbon nanotube, the density of states become not circularly uniform along the system.

From Figure 3-4(d) it is observed that more density of states are located at the larger curvature part of the carbon nanotube. In comparing Figure 3-4(a) and (b) with Figure 3-4(c) and (d), we can find that the density of states increases significantly. It can be explained that more copper chains encapsulated in the system the more free electrons introduced into the system.

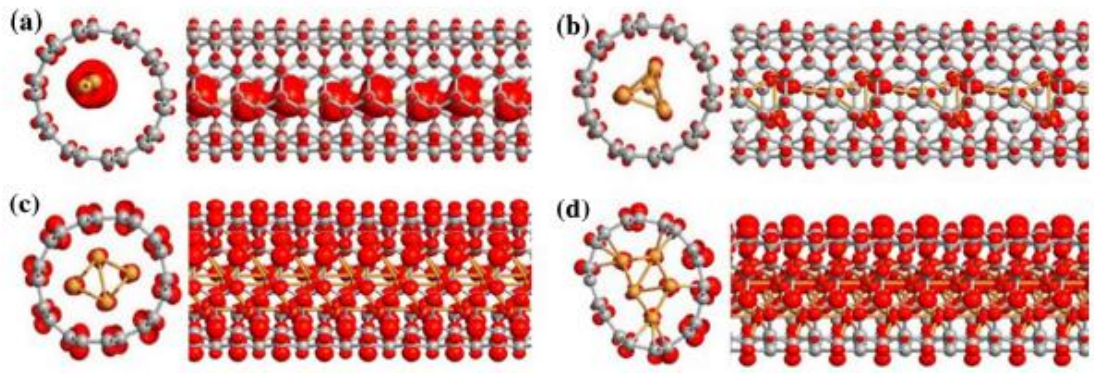

Figure 3-4 Local Density of States configuration of CNT (5, 5)-Cu system with (a) one Cu chain; (b) two Cu chains; (c) four Cu chains; and (d) five Cu chains encapsulated.

3.3.4 Mulliken Population

For a better insight of the interaction between copper chains and the carbon nanotube, Mulliken population analysis is carried and results are presented in Table 3-1. The Mulliken population of

electrons of atoms is associated with the bonding nature between atoms. The charge transfer from copper atoms to the carbon nanotube exists in all the four systems studied.

Table 3-1 Mulliken population of different CNT (5, 5) - Cu systems

Table I. Mulliken population of different CNT (5, 5)-Cu systems

	Mulliken population of Cu (e)	Mulliken population of CNT (e)
CNT (5,5)-1Cu	−0.05738	0.003388
CNT (5,5)-2Cu	−0.01519	0.001956
CNT (5,5)-4Cu	−0.00684	0.0015
CNT (5,5)-5Cu	−0.00233	0.000744

The Mulliken population of carbon atom is increased by 0.003388e when 1 copper chain is encapsulated by CNT (5, 5). With more copper chains encapsulated in the system, the increment of the Mulliken population of CNT is smaller. When 5 copper chains are involved in the system, only 0.000744 increase of Mulliken population of CNT is found. Accordingly, the Mulliken population of copper atom decreases as that of CNT increases. The loss of Mulliken population for Cu atoms has a range from 0.00233 to 0.05738. In all cases the Mulliken population change of both carbon and copper atoms is less than 1%. Therefor there are no chemical bonds formed between carbon and copper atoms which are consistent.

Table 3-2 Transmission coefficient at Fermi level of CNT (5, 5) with one, two, four and five Cu chains.

Table II. Transmission coefficient at Fermi level of one, two, four, and five copper chains—CNT (5, 5)

	CNT	Cu	CNT-Cu
One chain	2	0	3
Two chains	2	0	3
Four chains	2	2	3
Five chains	2	2	5

3.3.5 Transmission Spectrum

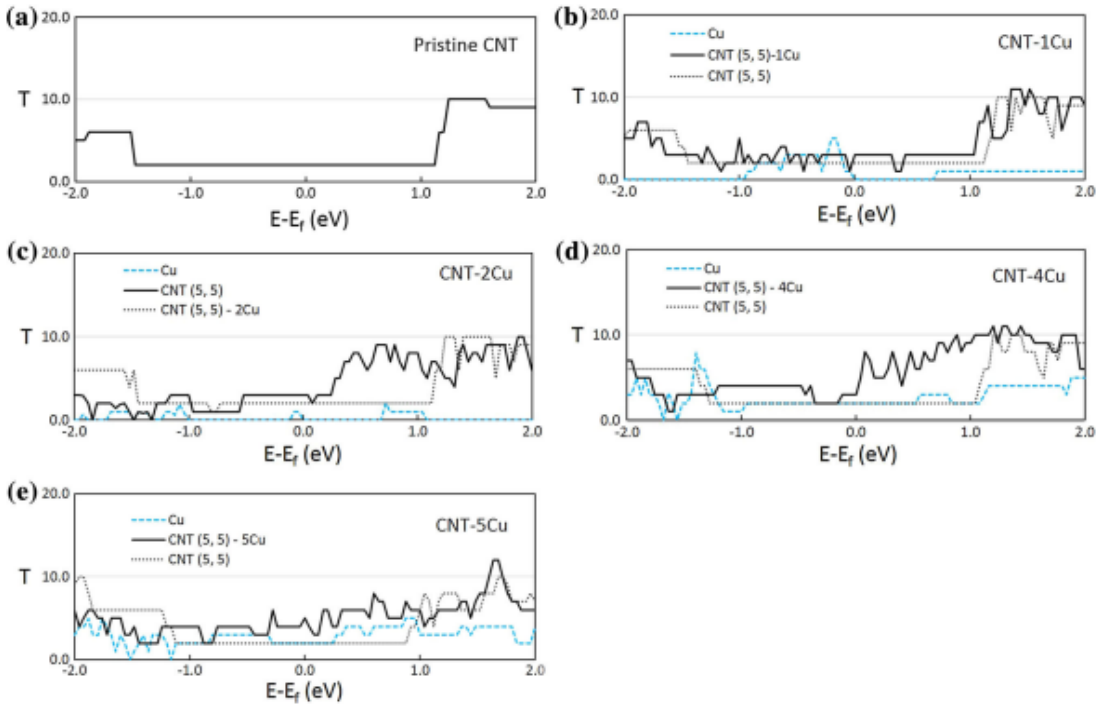

Figure 3-5 Transmission spectrum of (a) a pristine CNT (5, 5) and CNT (5, 5) –Cu system with (b) one Cu chain; (c) two Cu chains; (d) four Cu chains; and (e) five Cu chains encapsulated.

The transmission spectrum at zero bias for pristine CNT (5, 5), CNT (5, 5)-1Cu chain, CNT (5, 5)-2Cu chains, CNT (5, 5)-4Cu chains and CNT (5, 5)-5Cu chains are presented in Figure 3-5. The black line is for whole system, blue lines and red lines in Figure 3-5 indicate the transmission spectrum of copper and the CNT (5, 5) respectively. The transmission spectrum for the pristine CNT (5, 5) is provided in Figure 3-5(a) for comparison. In comparison of the hybrid system with the pristine CNT, some small peaks and dips around the Fermi level are observed in Figure 3-5 and it indicates the interaction of CNT and copper chains as well. The transmission coefficient T is equal to 2 for the pristine CNT (5, 5) as shown in Figure 3-5(a). CNT-1Cu hybrid system has a transmission coefficient equal to 3 at the Fermi level and with more copper chains encapsulated, it stays at 3 until 5 copper chains are encapsulated that the value of transmission coefficient turns to 5 at Fermi level. The transmission coefficient of CNT (5, 5), copper chains and CNT (5, 5) - Cu hybrid system at Fermi level are shown in

Table 3-2. The coefficient of the hybrid system is not equal to the sum of CNT (5, 5) and the copper chains. It indicates that the interaction between CNT and copper chains can be positive or negative for the system's conductance. CNT-Cu hybrid system of 1, 2, and 5 copper chains have greater T values than the summation of that of CNT (5, 5) and copper chains. However, for the case of 4 copper chains encapsulated CNT (5, 5), it is lower. The conductance of a nanowire system can be known as a function of transmission probability for each channel of the nanowire. So, the conductance of a ballistic system could be calculated by Landauer formula [39] :

$$G = G_0 * T \tag{3-2}$$

Where, $G_0=2e^2/h=1/12.9k\Omega$, T is the transmission coefficient of the system at Fermi level. Authors did the calculations on electronic and transmission analysis of different system with 4 unit cells, 6 unit cells, and 10 unit cells. The results show that the transmission coefficient at the Fermi level are the same. Thus the constructed system is ballistic. The total conductance of pristine CNT (5, 5) is $2G_0$ and that for CNT (5, 5) - 1, 2, 4 chains is $3G_0$, and $5G_0$ for CNT (5, 5) – 5Cu chains system. Based on this the interaction between Cu and CNT for 1, 2, 5 copper chains involved system improves the system's conductance and Cu-4CNT interaction impedes the transmission and lower the total conductance of the system.

The conductance of the CNT (5, 5) has been increased by encapsulation of copper chains. However, the enhancement is dependent on the number of copper atoms and it is probably related to the deformation of carbon nanotubes. With more copper chains inside carbon nanotube the deformation becomes larger and the deformation leads to a smaller gap in density of states. It looks that for one and two copper chains the conductance of the CNT be increased by 50%.

3.4 Conclusion

The density functional theory with NEGF method is applied to study the electronic and transport properties of armchair CNT (5, 5) encapsulated with 1, 2, 4 and 5 Cu chains. The binding energy of copper encapsulation CNT (5, 5) is relatively lower compared with other normally used electronic metals. The copper-CNT interaction did not form a bond between them. However, the

interaction lowers the gap in Density of States of the carbon nanotube around the Fermi level, as well as enhances the systems' the density of states around Fermi level. The LDOS isosurface shows that the deformation leads to a different distribution of electrons on the carbon nanotube that the larger curvature has a larger LDOS value. The copper encapsulated CNT (5, 5) hybrid system has a greater conductance than the pristine CNT (5, 5) and with 5 copper chains in the system the conductance can be improved by 250%.

CHAPTER 4 : ELECTRONIC STRUCTURE AND TRANSPORT PROPERTIES OF CARBON NANOTUBE ADSORBED WITH ALUMINIUM

4.1 Introduction

The growing demand on decreasing the minimum feature size to decrease the cost of circuits in semiconductor industry has pushed the use of conventional conductive material (mainly copper and aluminum) as interconnects to their limits since the electrical resistivity of these metals are inversely increased with the linewidth when the feature size is less than 100nm. The consequence of the increased resistivity includes the increased power loss due to Joule heating, severs electromigration as well as significantly increased budget for the thermal management [40]. The increased resistivity in nanoscale is mainly attributed to the down-scaling in metal conductors caused severe surface and grain boundary scattering, especially when the feature size of metal interconnects is less than the mean free path for electrons.

Recently carbon nanotubes (CNT) have been regarded as an alternate nanoscale conductor to replace copper as interconnects, mainly due to their remarkable properties, e.g. high current carrying capacity [41], ballistic transport [42], low density, and high strength and stiffness [43-45], plus they have much larger (about a factor of 1,000) mean free path than copper. However, due to the limited free charge (electrons and holes) density, carbon nanotubes have a conductivity which is only close to or comparable to that of copper in nanoscale, and interconnects in nanoelectronic require significantly lower resistivity to reduce the RC delay. In addition, nanoscale electrodes with lower resistivity are also needed for biomolecule and biomedical applications to significantly reduce the negative effects due to Joule heating.

Novel hybrid materials containing carbon nanotubes and metals can potentially improve a number of properties of conventional conductors but one important area would be to allow them to transmit current more efficiently with low resistivity. Copper was used to decorate CNT to form a novel 1-dimensional hybrid nanowire which combines the synergistic properties from both CNT and metallic nanowire [35]. It has been reported that the adsorption of a Titanium chain onto carbon nanotube can significantly modify the electronic structures around Fermi energy for carbon nanotubes [46]. The conductance of both semiconducting and metallic carbon nanotube was improved with the adsorption of copper nanowire [36, 47]. Aluminum, with only one valence

electron in the 3p shell, is more likely to have stronger interaction with carbon nanotube than copper which has nearly filled outer sd shells[46]. Besides, Al has 3 valence electrons which is three times more than copper does. In this paper, the studies on hybrid nanowire consisting of CNT and aluminum with emphasis on electron transmission are carried and the results are presented. The CNT considered here is semiconducting type in CNT (10, 0).

4.2 Calculation Method and Simulation Model

To compute the electron transport in CNT-Al hybrid material, a two-probe system was constructed by dividing the CNT-Al hybrid wire into three regions, namely, left-electrode (8.5 Å), right-electrode (8.5 Å) and the central scattering region (34.1Å) in between the electrodes. A region of vacuum space which is sufficiently large so that we could consider the CNT as an isolated individual one is generated around each electrode. The configuration of a hybrid system of nanotube and 10 Al chains adsorbed is shown in chains Figure. Cartesian coordination system was applied in the calculation and the tube's axial direction was set as the z-axis. The central scattering region consists of 8 unit cells of CNT (10, 0)/Al and each unit cell is optimized with Density Functional Theory (DFT). The local density approximation (LDA) [38] with double zeta basis sets was used in the geometry optimization. For the two probe system analysis, the general gradient approximation (GGA) was applied. For convergence, a tolerance of $1*10^{-5}$ Hatree of total energy was used as the criterion. The Brillouin zone parameter was set to as 1*1*100. All the computations were performed using the commercial software package QuantumWise (ATK-13.8.1). The results for CNT (10, 0) adsorbed with 1Al-chain, 2Al-chains, 4Al-chains, 6Al-chains, and 8Al-chains will be presented first and it will follow the results of CNT (10, 0) adsorbed with 10Al-chains, in which the whole CNT(10,0) surface was covered by aluminum chains.

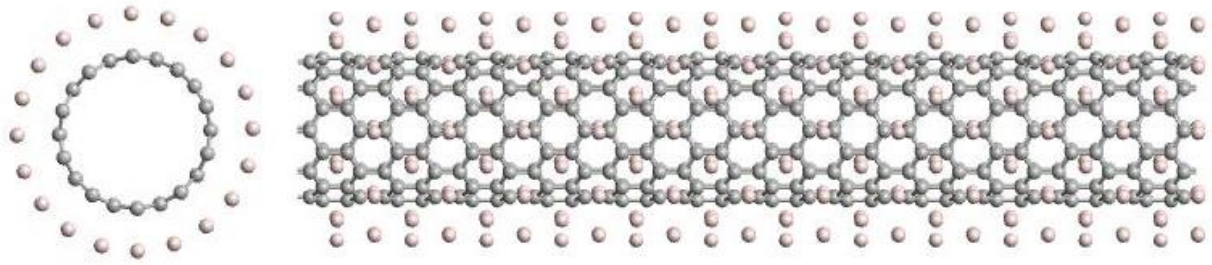

Figure 4-1 The side (left) and top (right) view of the configuration of CNT (10, 0) adsorbed with 10 Al chains.

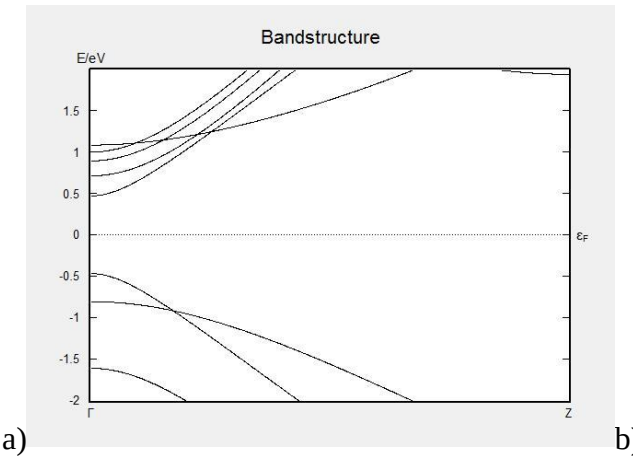

a)

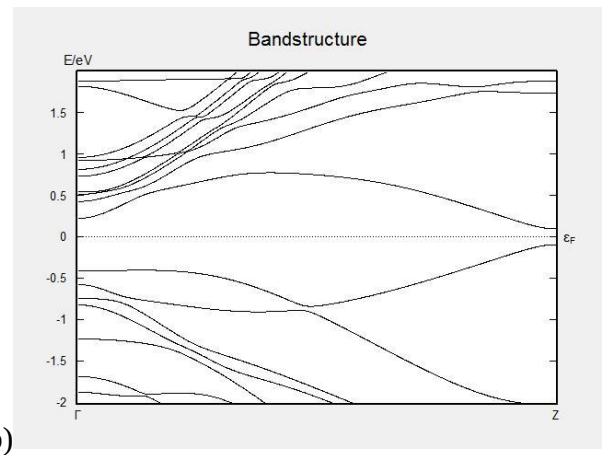

b)

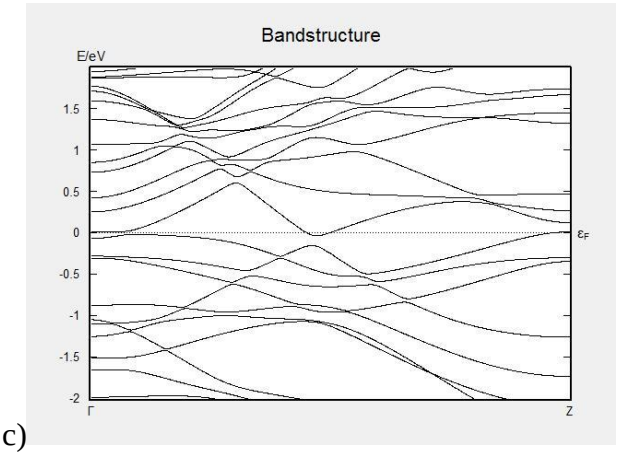

c)

Figure 4-2 The band structure of a) pure CNT (10, 0); b) CNT (10, 0) adsorbed with 1 Al chain; c) CNT (10, 0) adsorbed with 4 Al chains.

4.3 Results and Discussion

4.3.1 Band Structure and Density of States

Figure 4-2 shows the band structures calculated for pure CNT (10, 0) and the hybrid material of CNT (10, 0) adsorbed with Al chain(s). The pure CNT (10, 0) is a semiconductor with small gap equal to 0.91eV which is larger than the results studied by zone-folding model [48]. In ref [48], it predicted the bandgap of CNT (10, 0) would be 0.82eV. In the zone-folding model, it neglects the curvature effect. And CNT (10, 0) has a diameter of 7.961 Å where the curvature effect would strongly influence the bandgap. Our calculated band structure agrees well with more accurate direct calculations performed with the CASP program package in ref [49]. The gap between valence band and conduction band is reduced to 0.638eV when an Al chain is adsorbed onto CNT (10, 0). And 4 adsorbed Al-chains, however, closes the band gap and effectively transforms the semiconducting SWNT into a metal, as denoted in Figure 4-2c. Figure 4-3 shows the density of statues (DOS) and Figure 4-3(a) shows the gap of 0.91eV for the pure CNT (10, 0). Figure 4-3(b) indicates the DOS of a free standing Al chain, and Figure 4-3(c) displays the density of states (DOS) for the 1Al-chain absorbed CNT(10,0) in which the bandgap has been reduced that It is related to the fact that Fermi level has been shifted toward to the conduction bands of the carbon nanotube. Similar behavior was reported for a single copper chain wrapped in a carbon nanotube [50]. 2Al-chains absorbed CNT (10, 0) has an even lower gap of 0.618eV. Noticeably, the high density of states around Fermi level shown in Figure 4-3(d) could well explain the metallic behavior for the 4 Al adsorbed CNT (10, 0) hybrid system. By the semiconducting theory, when Aluminum atoms are adsorbed onto the semiconducting CNT, the excess electrons from Aluminum must reside in the conduction bands in order to retain the overall system as charge-neutral. Therefore, with more extra electrons which comes from Al atomic chains, the Fermi level would shift more toward the conduction band and finally resides in the conduction bands. In another word, the conduction band energy becomes lower and lower when more aluminum atoms are adsorbed onto the semiconducting CNT (10, 0).

4.3.2 Electron Density

In order to further understand the electronic states around the Fermi level and the interaction between Al and nanotube (10, 0), the isosurface for the electron density of four bands that are

closest to the Fermi level of the hybrid CNT(10,0)/Al system are analyzed and results are presented in Figure 4-4. As shown in Figure 4-4(a), the electrons from these bands are delocalized and redistributed on both aluminum and its closest carbon atoms in the hybrid system of nanotube (10, 0) adsorbed with 1 Al chain. Similar behavior was observed for the hybrid system with 4 Al chains. Whereas for the 4-Al chains absorbed hybrid system, the electron density almost covered all over nanotube instead of covering partially as in the case of 1Al chain absorbed hybrid system. Detailed analysis results on the partial electron local density of states indicate that the DOS at Fermi level for the 4 Al chains absorbed hybrid system are composed of p electrons from aluminum and p electrons from carbon.

4.3.3 Transmission Spectrum and Eigenstates

To help in understanding the conductance physics of the hybrid systems, transmission eigenstates which could provide a direct picture of the electronic states that contribute to the conductance were also investigated. For CNT (10, 0)/4Al system there are 3 transmission eigenchannels could be observed. And all of them are located both on Al and C atoms. The first two channels are related to the same two Al chains and their nearby carbon atoms on the nanotube. Another channel is formed with the other two Al chains and their nearby carbon atoms. This is in consistency with charge density of HOMO and LUMO bands of the system. We could find that the charge density was located all over the 4 Al chains and their nearby C atoms on the nanotube in the HOMO band. However, for the LUMO band, only the two Al chains that are associated with two transmission channels have charge density all over them and their nearby C atoms. Much less charge density could be observed around the other two Al chains. It could explain that two transmission eigenchannels formed with the first two Al chains and only one transmission egienchannel on the other side.

The transmission spectrum of CNT (10, 0) absorbed with 10 Al chains hybrid system is presented in Figure 4-6. The transmission coefficient of the CNT (10, 0)/10Al hybrid system is 14 at Fermi level, indicating the metallic behavior of the system. Since the transport is ballistic here, the transmission coefficient could be achieved from band structure as well. The band structure shows that 14 bands going across the Fermi level, which agree with the results of transmission spectrum.

Further study can find that each of the 14 transmission eigenchannels of the hybrid system is related to both Al and C atoms. That indicates both the nanotube and metal chains are contributing to the conduction of the system. To be more specific, the large density of states around the Fermi level is consisted of both p electrons from aluminum and p electrons from carbon.

(a)

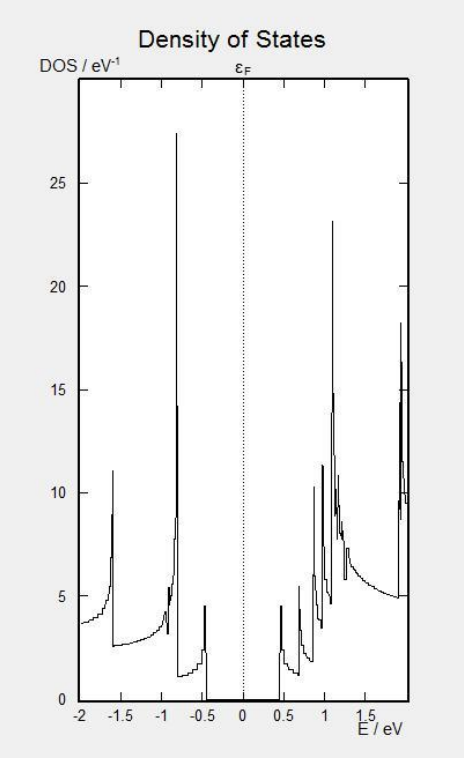

(b)

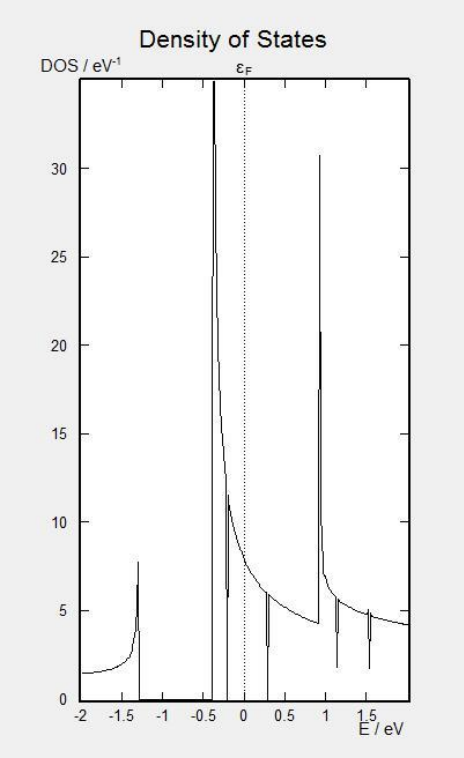

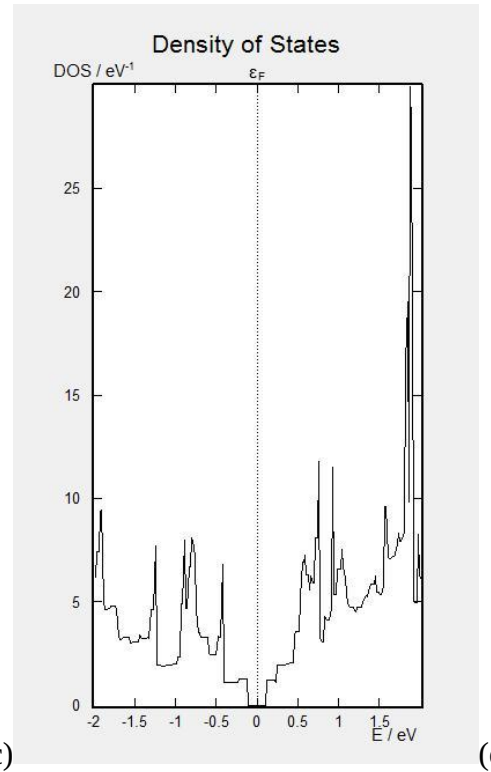

(c)

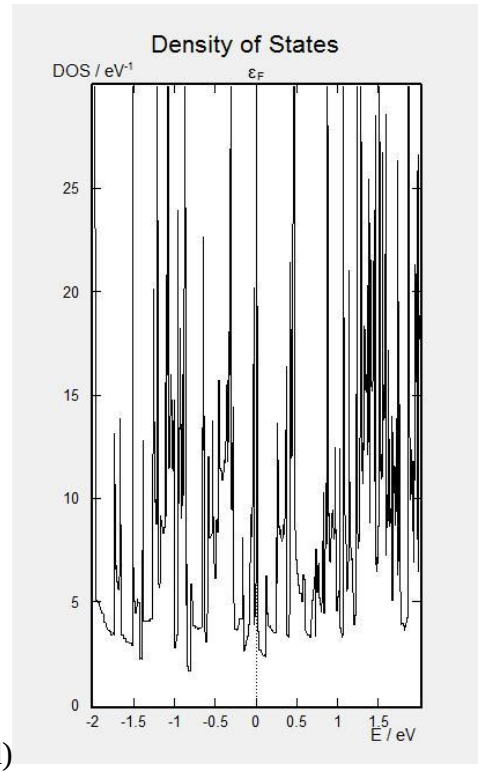

(d)

Figure 4-3 Density of states of (a) for pristine CNT (10, 0); (b) for a free standing Al chain; (c) for CNT (10, 0) adsorbed with 1 Al chain; (d) for CNT (10, 0) adsorbed with 4 Al chains.

4.3.4 Conductance

As we know, for nanowires whose size is comparable to electron's mean free path, the transport would be ballistic and the conductance can be calculated via Landauer formula [15].

$$G = T(E_F)G_0 \tag{4-1}$$

Where T (E_F) is the transmission coefficient at Fermi level energy E_F and G_0 is the conductance quantum ($7.748091733*10^{-5}$ S).

It can be understood as the electronic transport through channels and could give the conductance limit of different systems where the temperature goes to zero. Here, we could calculate the zero bias conductance of the system at 0K is 1.0847 mS. In Figure 4-7, the I-V curve and conductance-voltage curve for the CNT (10, 0) absorbed with 10 Al chains system at elevated temperature of

300K is shown here. As it is stated above, in order to eliminate the contact resistance, the hybrid material itself were used as electrodes in the analysis. As reported [51-53], at low applied voltage regime (0.0-0.1V), the I-V relationship is linear. Thus, the total resistance of the system can be computed via Ohm's law. By averaging the data between 0 and 0.1V, the total electrical resistance of the hybrid system is 1.0874mS which is close to the conductance limit. In Figure 4-7(b), we calculated the conductance by integrating an energy range of transmission spectrum which are contributing to the thermionic emission. And a conductance value of 1.0844 mS is observed from Figure 4-7(b) when the system has no volt applied. In ref [54], the conductance of 0.7748 mS was reported for a perfect Cu nanowire with a diameter of 1.2nm. Hence the resultant conductance of CNT (10,0) adsorbed Al hybrid nanowire is about 40% greater than that of 1.2nm copper nanowire.

(a) 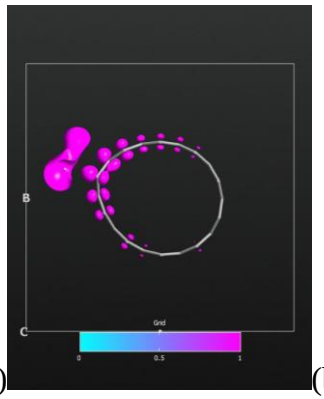 (b) 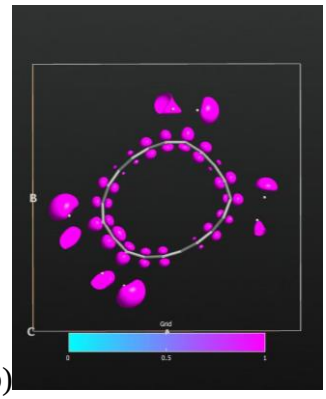

Figure 4-4 Isosurface for the charge density of the four closet bands around Fermi level of hybrid system (a) CNT(10,0) absorbed with 1 Al chain (isovalue =0.6); (b) CNT(10,0) absorbed with 4 Al chains (isovalue =0.3).

(a) 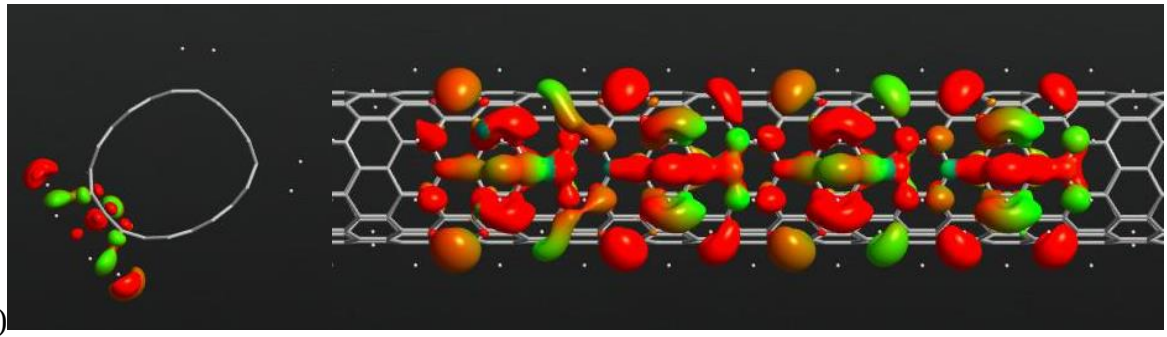

(b) 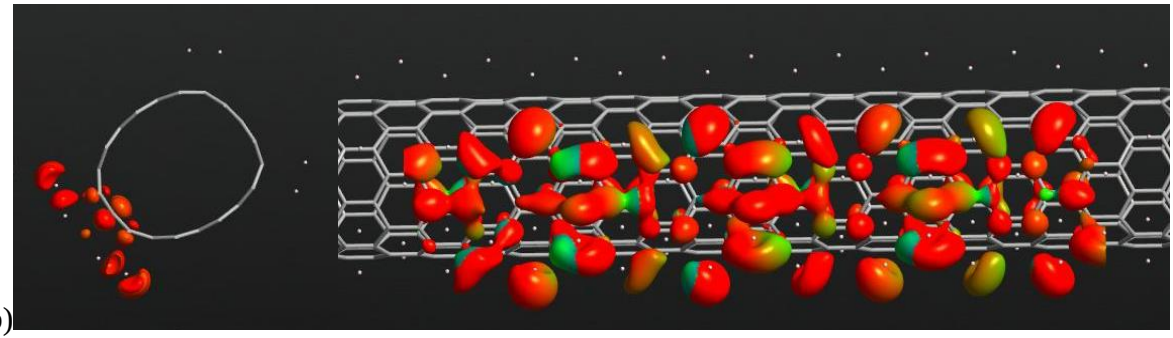

(c) 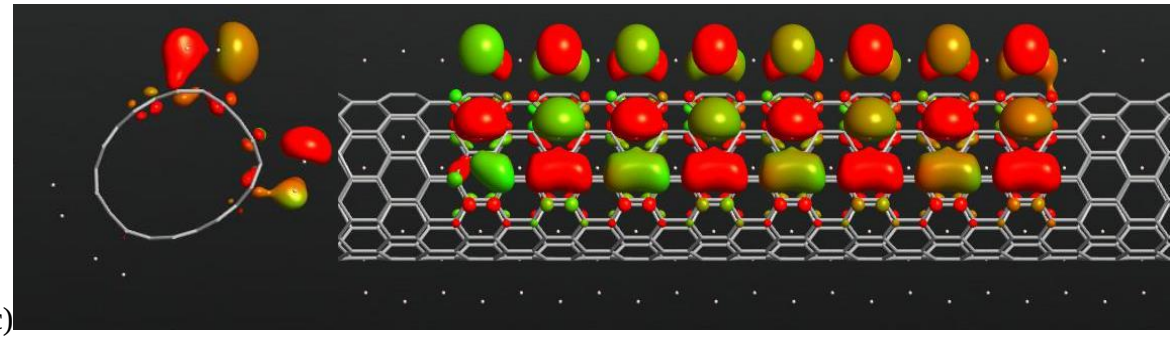

Figure 4-5 Isosurface for the 3 transmission eigenstates of hybrid system CNT (10, 0) absorbed with 4 Al chains.

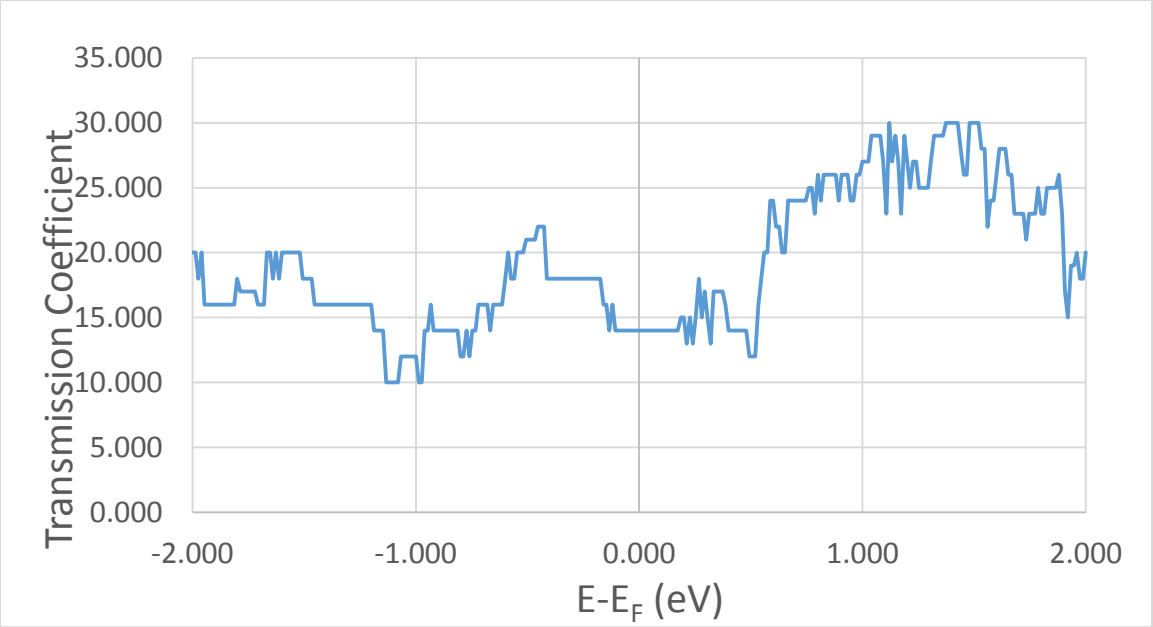

Figure 4-6 Transmission Spectrum of CNT (10, 0) adsorbed with 10 Al chains hybrid nanowires.

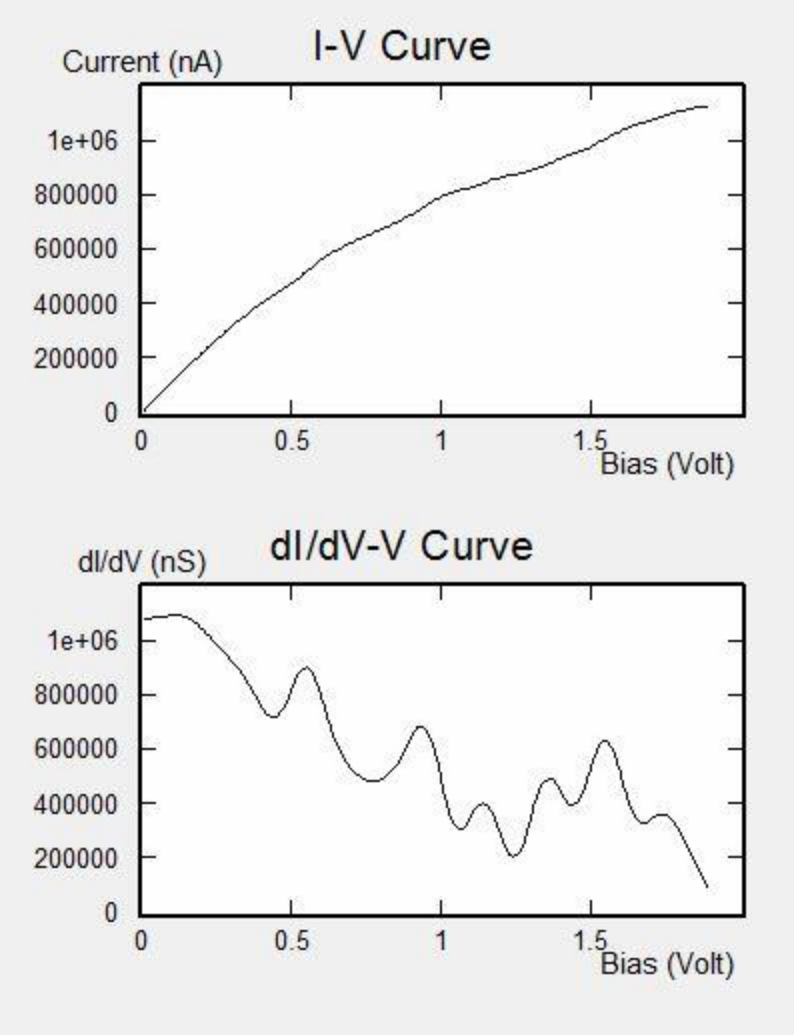

Figure 4-7 I-V curve (up) and Conductance-Voltage curve (down) for CNT (10, 0) adsorbed with 10 Al chains nanowires.

4.4 Conclusion

The hybrid nanowires made of semiconducting CNT (10, 0) absorbed with Al chains were studied with Density Functional Theory. The band structure and the Density of States results show that Al chains would reduce the band gap of nanotube which is transformed from semiconducting to metallic when four or more Al chains are adsorbed. Transport properties of CNT (10, 0) absorbed with 10 Al chains show that the hybrid system has a resultant conductance about 40% greater than that of pure copper nanowire of the same diameter. The relationship of conductance versus the applied voltage has also been investigated. These results suggest that CNT (10, 0)/Al hybrid nanowires could be used to replace copper nanowires as future nanoscale interconnects.

CHAPTER 5 : ELECTRICAL CONTACT RESISTANCE AT THE AL DECORATED CARBON NANOTUBE/AL INTERFACE IN END-CONTACT BY FIRST PRINCIPLE CALCULATIONS

5.1 Introduction

The use of conventional conductors in electrical wires and interconnects has been challenged due to the growing demand for electrical energy, rising cost and the need for carrying high power in nano sized devices. High resistance in these conductors causes serious performance issues such as reduced calculation speed, large power losses and reliability. Novel hybrid materials containing carbon nanomaterials could potentially improve a number of properties of conventional conductors, especially would allow them to transmit current more efficiently at a lower cost [55]. A carbon nanotube is obviously one of the promising candidate [56] that has ballistic transport [42] and is thermally and mechanically stable while carrying high current densities [41].

It has been reported that an individual semiconducting CNT can operate either as a conventional metal-oxide semiconductor field effect transistor [23, 57] or an unconventional Schottky barrier transistor [58] when it makes a contact with a metal electrode [59]. Therefore, the interaction between a CNT and its metal end and the resultant electronic properties like contact resistance are crucial. Numerous studies have been reported on metal electrodes forming end-contact, embedded-contact and side-contact with CNTs [51, 52, 60-64]. Among these, the end-contact between CNTs and electrodes which showed a low contact resistance in interfaces comparing with that for side-contact device [65] is often practical in potential electronic interconnects. Recent research has shown that the total resistance in end-contact system is attributed to the contact resistance at the CNT and the metal interface because bulk resistance of the metal probe is negligible [53]. Thus, to reduce the contact resistance between CNT and metal electrode is gaining more attention from industry. Meanwhile, various metals such as Cu, Ti, Al, Au and Ni, have been used to decorate CNTs. The electronic structures of these hybrid system have also been presented [36, 46, 47, 66-68]. However, few studies have been published on end-contact between metal electrode and metal decorated CNT. The interaction and electron transport properties need to be fully studied. In this paper, the local structure of metal decorated CNT was first optimized and then it was used to build whole system. Transmission spectrum, Mulliken Population, Density of States, I-V characteristics

and contact resistance from first principles calculations were reported here to investigate properties of the device.

5.2 Theoretical Approach and Model

A two-probe system was constructed that consisting of three regions, namely the left-electrode, the right-electrode and the central scattering region as shown in Figure 1(a). The two metal (Al) electrodes are treated as bulk systems and therefore are constructed as such with 5*5*4 atoms. The central scattering region located between the two Aluminum probes consisted of 2 unit cells of hybrid CNT-Al connected to six surface layers of Aluminum atoms on both sides. These Aluminum layers were considered as extension of electrodes providing screening, so that the scattering of Aluminum decorated nanotube is not presented inside the actual electrodes. This fundamental assumption in the two probe algorithms used here makes the electronic structure of electrodes bulk-like, although the electron density around the Aluminum layers may be perturbed by the Aluminum adsorbed nanotube. This perturbation, however, would decay towards the bulk density as it approaches to the electrodes on both sides. Each unit cell of CNT-Al was optimized with Local Density Approximation (LDA)[38] as exchange-correlation functional in Density Functional Theory (DFT) containing one CNT (10, 0) adsorbed with 10 Al chains. The configuration of one unit cell is shown in Figure 1(b) (c). The separation distance between decorated CNT and the metal (Al) surface was determined by minimizing the interaction energy of the system. The General Gradient Approximation (GGA) with Perdew-Burke-Ernzerhof (PBE) pseudoatomic potentials [69] was applied to DFT to analyze the local density of states near the CNT/metal interfaces. In conjunction with DFT, a no equilibrium Green's function method was used to calculate the transmission coefficient. The first-principles simulations were done with the ATK ToolKit 13.8.1 package.

An electrical voltage is prescribed across the two-probe system to generate a steady-state current in order to conduct the analytical studies. The electrons transport through the device along axial is denoted as the z direction and the other two orthogonal directions are denoted as the x- and y-directions. And the current-voltage relation of the system was obtained by using the landauer-Buttiker formula, from which the contact resistance can be determined.

5.3 Results and Discussion

5.3.1 Device Configuration

Three devices were built and analyzed which are shown in Figure 2. For devices built with CNT-Al, it was laid between the screening Al layers longitudinally and transversely. And a longitudinal pristine CNT device was built for comparison as well.

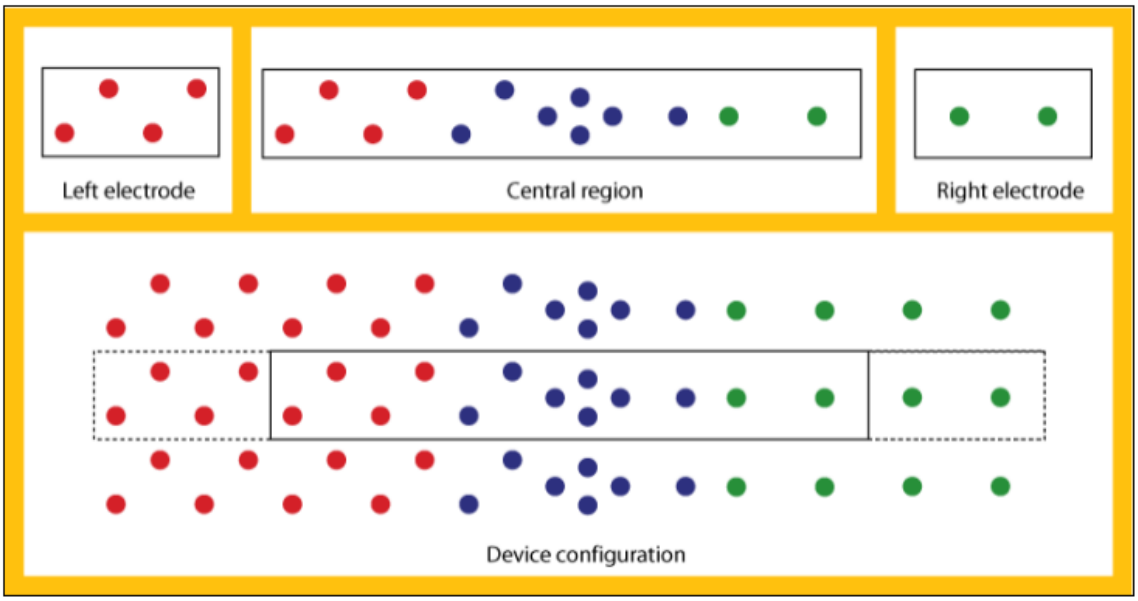

(a)

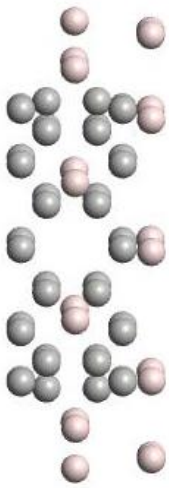

(b)

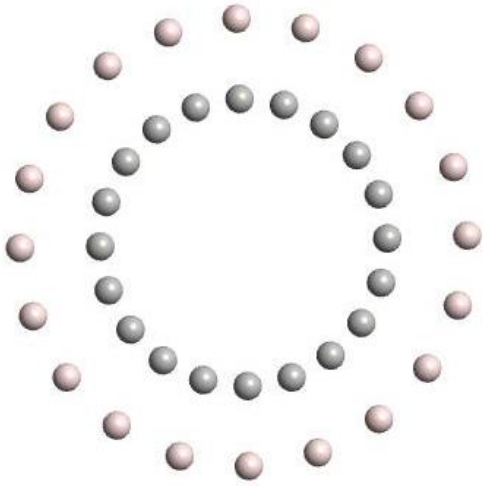

(c)

Figure 5-1 (a) a schematic two probe device[70], (b) lateral view and (c) side view of a unit cell of 10 Al chains adsorbed CNT (5, 5).

5.3.2 Mulliken Population

The Mulliken population of the three two-probe systems were computed to characterize the bond between the center part and Aluminum electrodes. And to separate the electron density from atomic contributions, the Mulliken overlap population (MOP) between atoms for a particular orbital was then extracted to reveal the bonding characteristics qualitatively [71]. Only the scattering region that includes CNT-Al and layers of metal surface was shown in the Figure 3. Thicker lines represent higher bond strength. It was seen that for both longitudinal and transverse CNT-Al systems, bonding was formed between Al atoms and Al metal layers. It could explain that we previously reported that CNT-Al systems had a higher probability for electrons to go through than that for CNT system did. Furthermore, chemical bond was found at the interface of longitudinal CNT-Al system between C and Al, which was in consistence with the result that longitudinal CNT-Al had a larger transmission coefficient at Fermi level than transverse CNT-Al system.

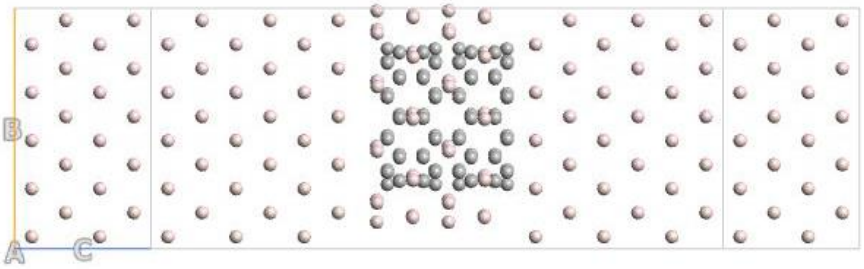

(a)

(b)

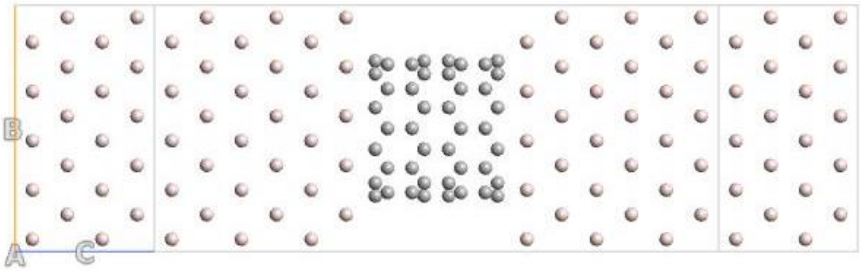

(c)

Figure 5-2 Two-probe system consisting of Al electrodes and center part of (a) a longitudinal CNT (10, 0), (b) a longitudinal CNT (10, 0) adsorbed with 10 Al chains, (c) a transverse CNT (10, 0) adsorbed with 10 Al chains.

5.3.3 Transmission Spectrum at zero bias

The calculated transmission spectrum at zero bias for the two probe system with CNT (10, 0) adsorbed with 10 Al chains longitudinally and transversely located in the central region were presented. For comparison, the transmission spectrum at zero bias for pristine CNT (10, 0) located in the central region longitudinally was also calculated. Figure 4 showed that the electron transmissibility decreased as longitudinal CNT-Al > transverse CNT-Al > longitudinal CNT, particularly around Fermi level. It was also observed that the Transmission coefficient was always

not quantized at fermi level and elevated energy levels. Because the system is not perfect, the conductance is not quantized in integer steps of G_0 as expected from the Landauer formula $G=G_0T$, where T denotes the transmission probability for all modes. According to the Landauer formula, the conductance of the two probe system gained more conductance after the Al adsorption onto CNT because of the higher transmission coefficient was observed from Figure 4. To further understand the transport property at Fermi level, the k point dependent transmission contours were calculated and presented in Figure 5. The longitudinal CNT-Al device has its highest transmission coefficient near the Gamma point at zero bias voltage. And the transmission probability is largest around (0.0, 0.18) for transverse CNT-Al device. The transport for the longitudinal CNT-Al device at Fermi level Gamma point can be described with 49 transmission eigenstates. Among the 49 eigenstates, there are 17 major channels which have the eigenvalues larger than 0.1. However, for the transverse CNT-Al device, the number of major channels dropped to 6 at its highest transmission coefficient point. It also explained that why longitudinal CNT-Al device had a larger transmission coefficient at Fermi level with no bias voltage.

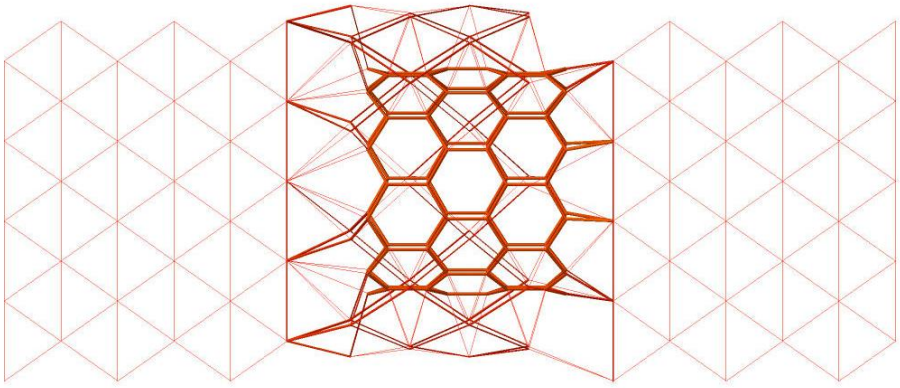

(a)

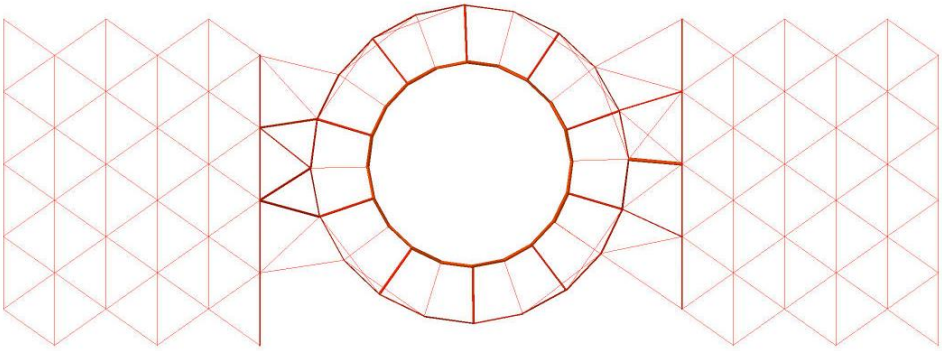

(b)

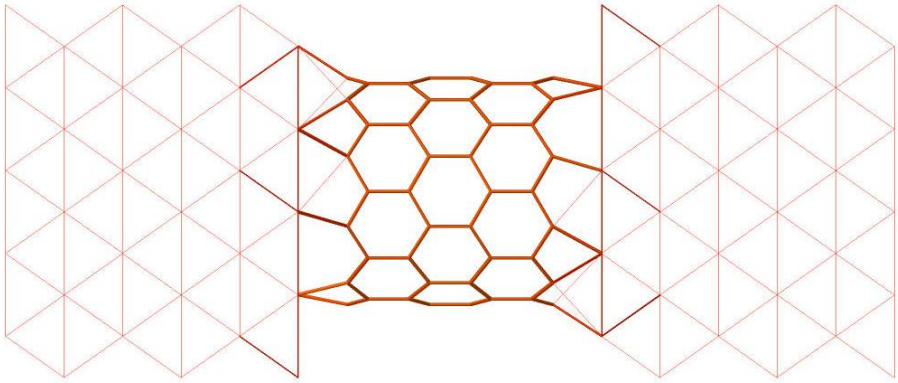

(c)

Figure 5-3 Mulliken Population for (a) longitudinal CNT-Al, (b) transverse CNT-Al, (c) longitudinal CNT.

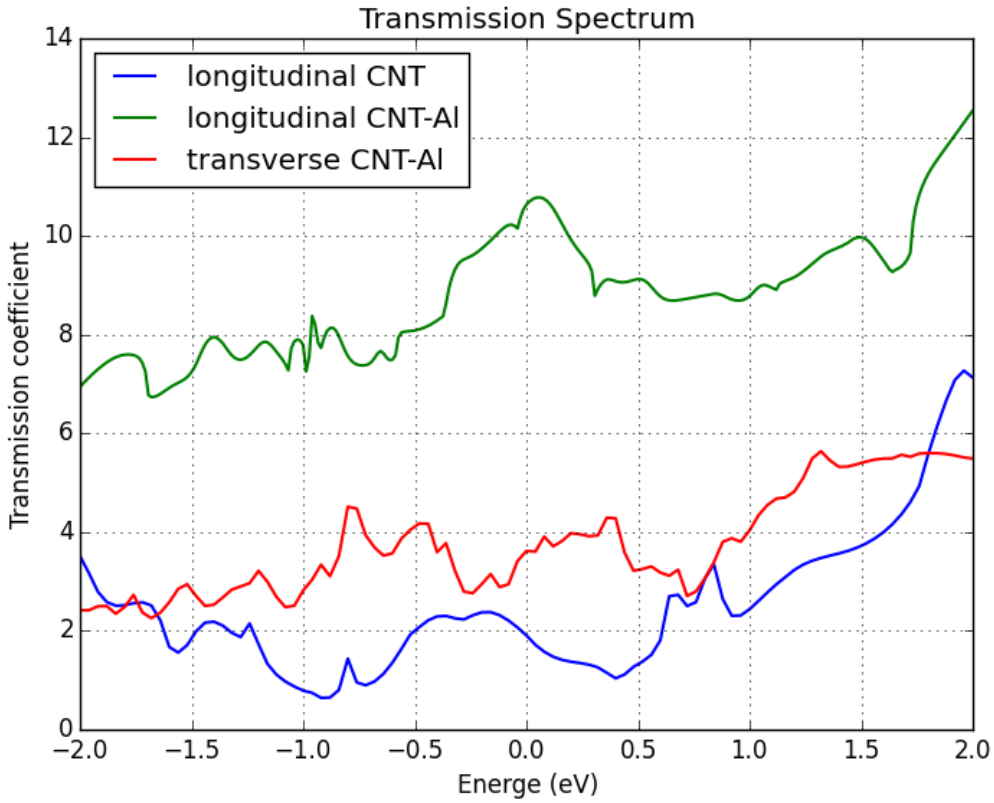

Figure 5-4 Transmission spectrum at zero bias for device of longitudinal CNT-Al, transverse CNT-Al, and longitudinal CNT.

5.3.4 Density of States (DOS)

In order to study the electronic structure at Fermi level which is crucial to the electron transport at the interface, the Local Density of States (LDOS) at Fermi level (E=0) were computed and showed in Figure 6. The contour was projected onto a cross-section parallel to the current flow direction of the two-probe device. It directly indicates the significant difference between the two probe systems. The states are located throughout C atoms along the tube axis for the longitudinal CNT adsorbed with Aluminum. Instead of the uniform states all over carbon atoms, for transverse mode most of the states sit on one end of the tube neck. This implies that more active electron transport in the longitudinal system than the transverse system. This conclusion was also confirmed by the previous transmission coefficient calculations.

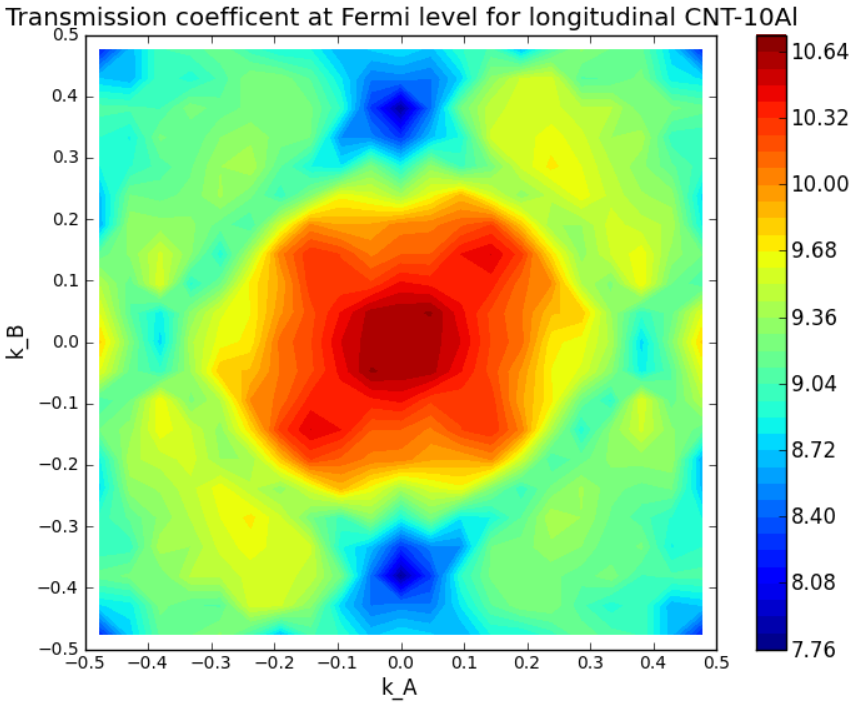

(a)

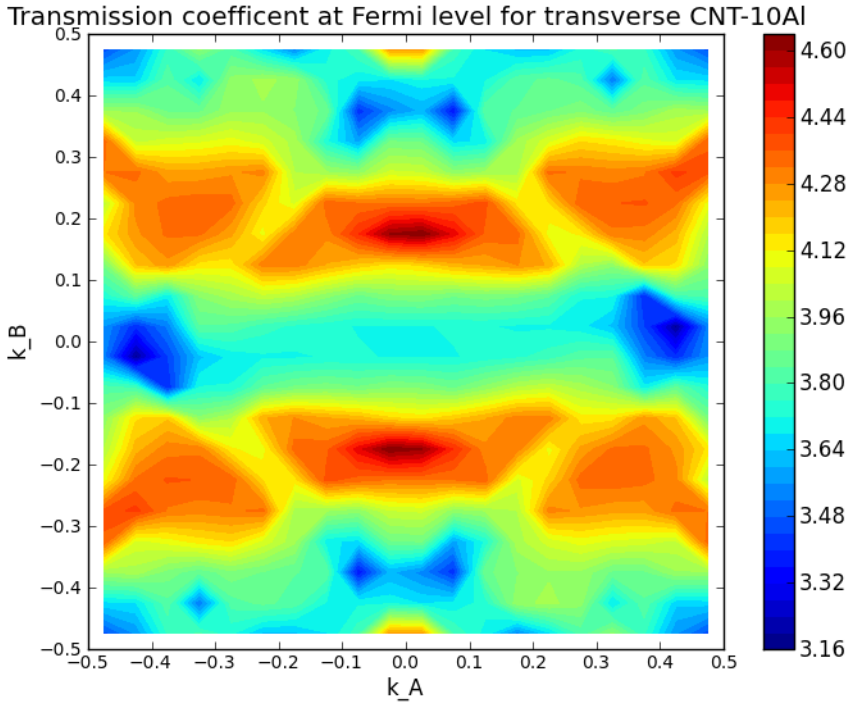

(b)

Figure 5-5 Transmission contour at Fermi level for (a) longitudinal CNT-Al (b) transverse CNT-Al.

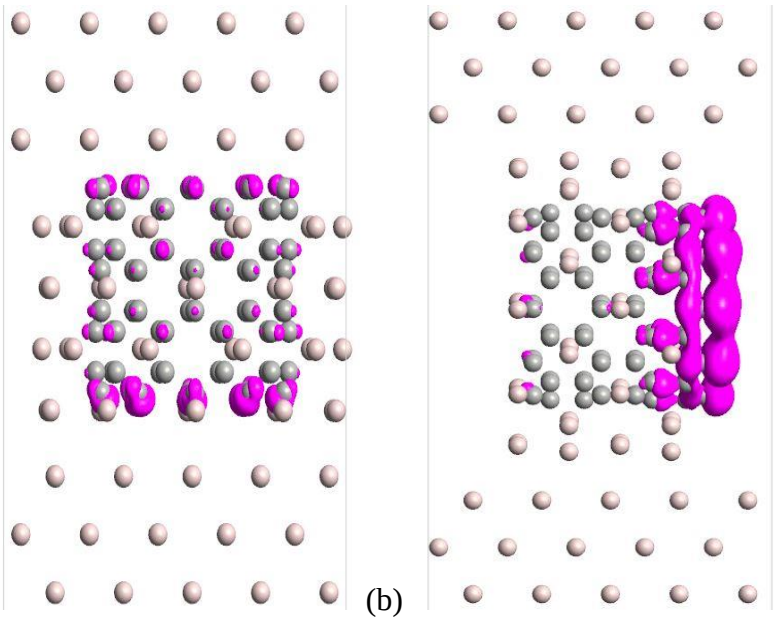

Figure 5-6 Local Density of states for two probe system with (a) longitudinal CNT-Al; (b) transverse CNT-Al. Note here three Al layers in the scattering region were shown in the figure.

5.3.5 I-V curve

The transmission spectrum at various bias voltages were calculated with the matrix version of the NEGF approach which is a well-developed general formalism to treat various no equilibrium charge transport phenomena. The k-point sampling in Brillouin Zone integration were 3*3*100 in the x-, y- and z-directions, respectively. The results are presented in Figure 7 where the transmission coefficient shows a strong dependence both on the applied bias voltages and energies for all the three two-probe systems. And because of this correlation, the linear response I-V curve by integration the transmission spectrum at zero bias in a wide bias interval were not used in this paper. Instead of using the build-in method of transmission spectrum to calculate the current, the current for I-V curve of Figure 8 were computed by the self-consistent transmission spectrum for each bias. Since the I-V relationship is linear at low applied voltage regime (0-0.1V), the total resistance of the system could be computed via the Ohm's law. Therefore, the electrical resistance for longitudinal and transverse model were 1.25 kΩ and 3.57 kΩ respectively. And for the longitudinal CNT two-probe device, the resistance was of 6.8 kΩ which is similar to the value reported by reference as 8.2 kΩ(*8*) for Al/CNT(10,0)/Al and 7.39kΩ for Al/CNT(5,5)/Al [72].

Also, according to reference [53], much of the total resistance in the metal/CNT/metal system is attributed to the contact resistance at the CNT/metal interfaces, because the total bulk resistance of the CNT and metal probes is negligible. Hence the contact resistance is respectively 0.625 kΩ and 1.785kΩ at each CNT+Al/Al interface for the longitudinal and transverse devices.

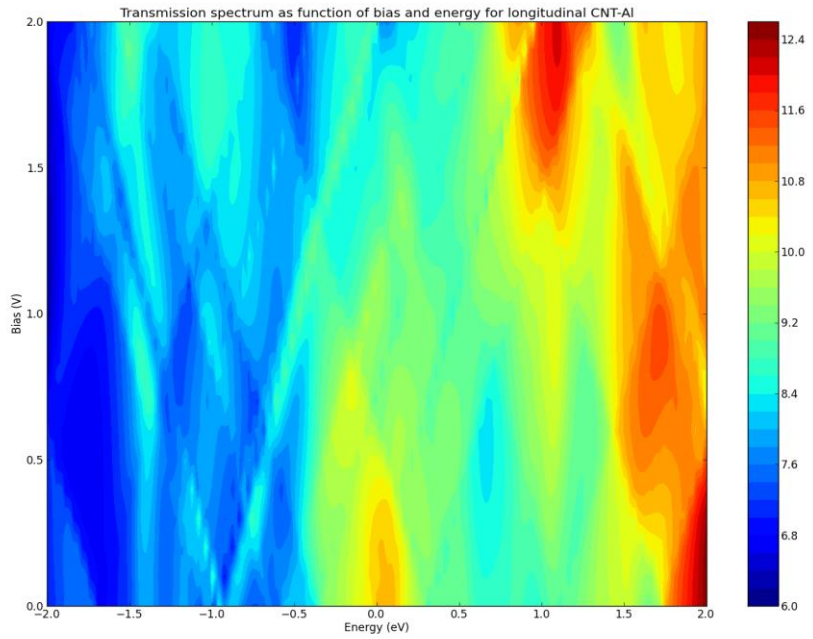

(a)

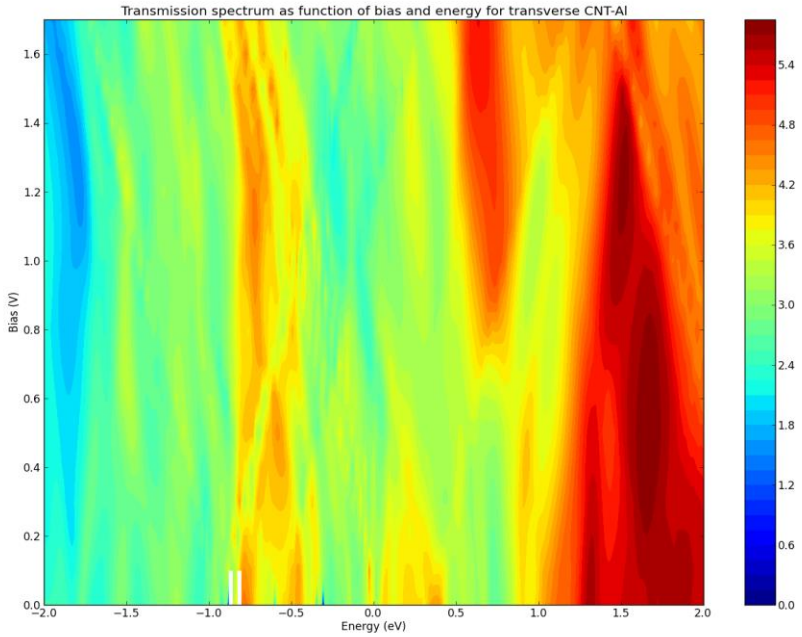

(b)

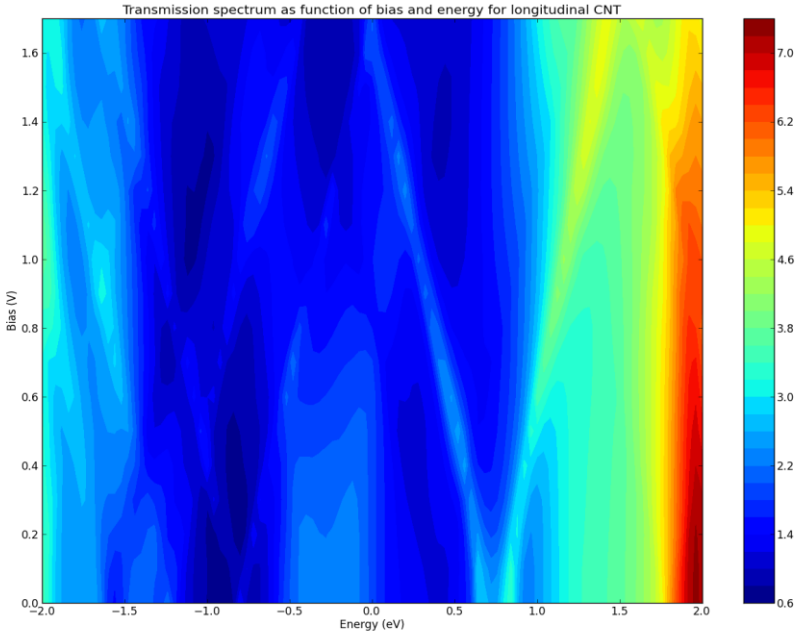

(c)

Figure 5-7 Transmission Spectrum as function of bias and energy for (a) longitudinal CNT-Al device, (b) transverse CNT-Al device, (c) longitudinal CNT device.

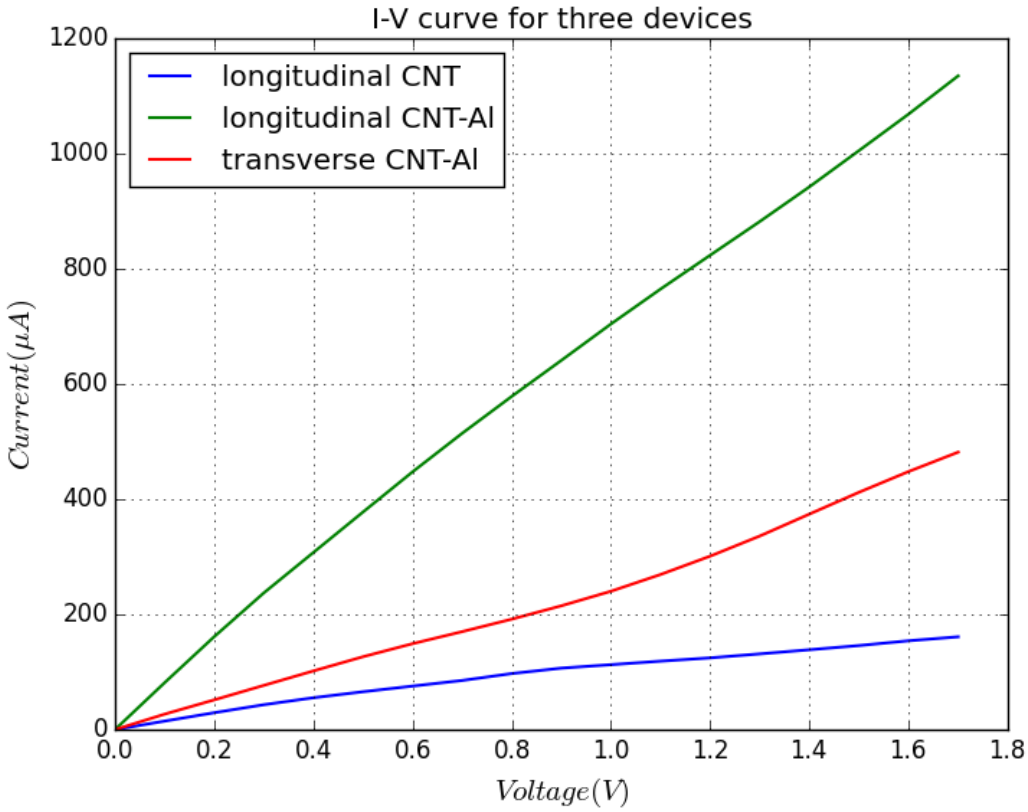

Figure 5-8 I-V curve for device of longitudinal CNT-Al, transverse CNT-Al, and longitudinal CNT.

5.4 Conclusion

Longitudinal and transverse Al decorated CNT (10, 0) were used to form end-contact with Al electrode. The transmission spectrum at zero bias showed that these devices had a good electron transporting property. Of the two devices, Al/longitudinal CNT (10, 0)-Al/Al showed lower contact resistance, which was about 1/3 of Al/transverse CNT (10, 0)-Al/Al and 1/10 of conventional Al/CNT (10, 0)/Al. It indicated the Al adsorbed CNT might be a good candidate to form end-contact devices.

CHAPTER 6 : ELECTRONIC STRUCTURE OF ALUMINIUM-DOPED CARBON NANOTUBES

6.1 Introduction

As the most important nanomaterial, carbon nanotubes (CNTs) distinguish themselves by their extremely small diameters, ultra long lengths, high chemical stability, outstanding mechanical properties and excellent electronic properties. However, defects in CNTs are inevitable and will influence the properties as some studies reported. The studies of doped CNTs, due to their interesting properties from both a fundamental physics as well as the possible applications viewpoint, were extremely active.

It is reported that impurities present in carbon nanotubes significantly affect their electronic and transport properties [73]. Devices have been proposed with compositions beyond that of pure CNTs and some of them have been experimentally realized. Nitrogen doped CNTs which make the tube surfaces chemically active facilitating chemical functionalization [74] could be a promising electrocatalysts candidate for oxygen reduction reactions in fuel cells and has been proven theoretically [75] and experimentally [76]. Unlike undoped tubes which exhibit a variety of metallic and semiconducting behavior depending on their chirality, it was observed that Nitrogen doped CNTs were all metallic and showed strong electron donor states near the Fermi level [77]. Moreover, studies of metal doped CNTs have been quite popular recently. Aluminum doped CNTs were expected to be a potential candidate for detecting the presence of carbon monoxide [78]. The Nickle doped CNTs could serve as a sensor for detecting oil-dissolved gases which improved the sensor response in Transformers [79]. Also researchers showed that Single walled CNTs doped with metals such as Potassium [80], Iodine [81] and Gold [82] [83] exhibit a conductivity enhancement. It was reported that pyridine-like N structures were responsible for the metallic behavior and prominent features of Nitrogen doped CNTs. [77] However, the effects of substitutional metal doped CNT has not been fully investigated since charge transfers were found in K doped CNTs where the doping did increase the carrier concentration and thus improved the conductivity. [84]Comparing to Potassium, Aluminum which has more valence electrons might be a prospective candidate to further enhance the conductivity of the doped CNTs. Therefore, the study on the effects of substitutional Al impurities on the property of SWCNT are reported in this paper.

6.2 Calculation Method and Simulation Model

In this letter, zigzag nanotubes (m, 0) with m=4-11 and armchair nanotubes (m, m) with m=4-6 are first calculated to study the diameter and helicity dependence of an Al-doped SWCNT. Each tube originally has 4m carbon atoms in the unit cell. And one of the carbon atom in the unit cell is replace with an Aluminum atom as shown in Figure 6-1 Optimized structure of Al doped CNT (10, 0)Figure 6-1. In order to study the doping rate dependence, the cases of a larger unit cell for SWCNT (10, 0) $C_{79}Al$ and two Aluminum atoms doping $C_{38}Al_2$ were studied, where the two Al atoms are placed so that Al-Al distance is maximized. Each unit cell is 16.78 Å * 16.78 Å along x and y axes which are large enough to avoid the intertube interactions.

All the calculations are carried out with the help of first principle calculations using QuantumWise(ATK-VNL) simulation package. The density functional theory (DFT) with the limits of local density approximation (LDA) with Perdew-Zunger (PZ) exchange correlation functional were utilized in all the models. Valence electrons are expanded in a double zeta plus polarized basis set for all atomic species. An energy cut-off of 75 Ha is set to present the accurate real space grid sampling. The sampling for Brillouin zone integration is performed with a grid of 1*1*100 k-points.

6.3 Results and discussion

6.3.1 Optimized structure and formation energy

Figure 6-1 illustrates the optimized structure of an Aluminum-doped (10, 0) carbon nanotube. Due to the fact that the Aluminum atom has a larger atomic radius than that of the carbon atom, the Aluminum atom in the optimized structure locates outside of the original atomic position in the pristine carbon nanotube to stretch the Al-C bond length. The tendency are the same for all of the Aluminum-doped tubes in this study. In the case of the (10, 0) tube, Aluminum moves outward from its original position by 0.98 Å, which is much smaller than that of graphene (1.43Å) [85]. This is because of the curvature of nanotube structure helps to reduce the strain needed to accommodate the Aluminum impurity. While the tube length barely stretches, indicating that the stretch of the Al-C bond length mainly gives rise to the change in the internal structures including

outward movement of Aluminum. Before doping, the calculated bond length for C-C in pristine CNT is 1.421 Å. For the Al-doped (10, 0) CNT, the nonequivalent lengths of Al-C bonds are 1.801 Å (axial) and 1.859 Å (diagonal). The Al-C bond length is close to the value 1.886 Å found in Al-Doped SWCNT (8, 0)[78] and that for Al doped graphene (1.85 Å)[85]. As a result, the distortion of the CNT is mainly limited to the first neighbors with only a small displacement for the second ones and the third ones are nearly unchanged. The diameter of (10, 0) CNT is 7.83 Å, while the minor and major of Al-doped SWCNT (10, 0) diameters are 7.50 Å and 8.47 Å respectively, changing the shape of the cross-section of nanotube from circular to slightly oval.

To discuss the stability of an Al-doped SWCNT, the formation energy of the substitutional Al impurity were calculated by the difference between the total energy of doped SWCNT to a pristine SWCNT as

$$\Delta E = E(C_{n-1}Al) - \frac{n-1}{n}E(C_n) - E(Al)$$

Where, E (C_n) and E ($C_{n-1}Al$) represent the total energies of a pristine and an Al-doped SWCNT respectively, and E(Al) represents the energy per atom in the α Aluminum. Figure 6-2 shows the result of ΔE as a function of diameter for Al-doped (m, 0) zigzag tubes $C_{4m-1}Al$, with m =4-11, and (m, m) armchair tubes, $C_{4m-1}Al$ with m =4-6.

The tendency can be observed that formation energy increases with the diameter in both zigzag and armchair tubes, indicating that narrower tubes are more energy favorable for Aluminum doping. It can be explained as follows: if an Aluminum atom is doped in a graphene layer which is the infinite diameter limit of the SWCNT, to stretch the Al-C bonds, carbon atoms would be pushed and Aluminum atom would move away from the graphene layer accompanied by symmetry breaking. Similarly, if an Aluminum atom is doped in nanotube, the Aluminum atom would move outward from the tube surface so that the symmetry would not be broken and Al-C bonds would be stretched. When the curvature is large, a small movement could be sufficient to stretch the Al-C bonds. Hence, it needs a relatively small energy to dope a substitutional Aluminum atom in a SWCNT with a large curvature. And the formation energy of Al-doped CNT (10, 0) is calculated as 4.307 eV which is similar to the formation energy of the Al-doped γ-graphene for $C_{105}Al_3$ is calculated around 4.327 eV.[86]For a given diameter, the formation energies of armchair CNTs

are always slightly smaller than those of zigzag CNTs suggesting that Al-doped armchair CNTs might be easier to obtain in experiment. It is similar to B doped graphene where B doped zigzag graphene has a larger formation energy than that of armchair graphene[87].

Figure 6-1 Optimized structure of Al doped CNT (10, 0)

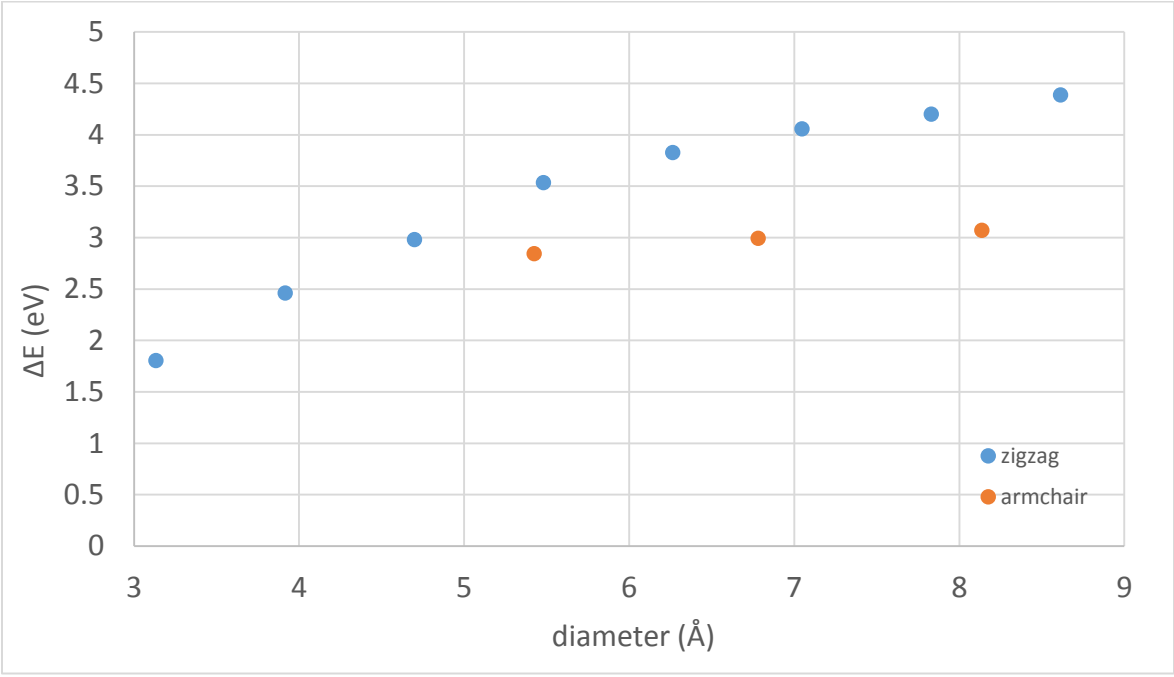

Figure 6-2 Formation energy as a function of nanotube diameter. (m, 0) zigzag tubes of m=4-12 (blue) and (m, m) armchair tubes of m=4-6 (orange) are plotted.

6.3.2 Band Structure and Density of States

The electronic band structure of a material serves as the signature for identifying its potential application in future electronic devices. Therefore, the band structures of the Al-doped carbon nanotubes (10, 0) were calculated to understand the electronic properties of optimized structures. Pristine CNT (10, 0) shows the significant band gap of ~ 0.896eV, which is in consistent with previous results in reference [88]. One or two boron atoms are substitutionally doped in unit of C_{40}, C_{80}. Figure 6-3 and Figure 6-4 respectively shows the electronic band structures and Density of states of C_{40}, $C_{39}Al$, $C_{79}Al$, and $C_{38}Al_2$. In all of the cases, the second highest valence band cross the Fermi level. And this band denote to the degenerate band of a pristine CNT (10, 0), whose degeneracy is lifted by Aluminum doping. An increasing Aluminum doping percentage will lead to a reducing band gap and a higher valence band maximum. The detailed values of valence-band maximum level and bandgaps are summarized in Table 6-1. Except for $C_{38}Al_2$, where Al dopants and nanotube bands mix together, the doped Aluminum atom creates a highly localized state that appears as a dispersionless band across the Fermi level in the band structure. And it accounts for a set of sharp peaks in the electronic density of states around Fermi level in Figure 6-4 (b) and (c). It is also observed from Figure 6-4 that the fermi level lies below the van Hove singularity at the edge of the valence band for all the doped nanotubes.

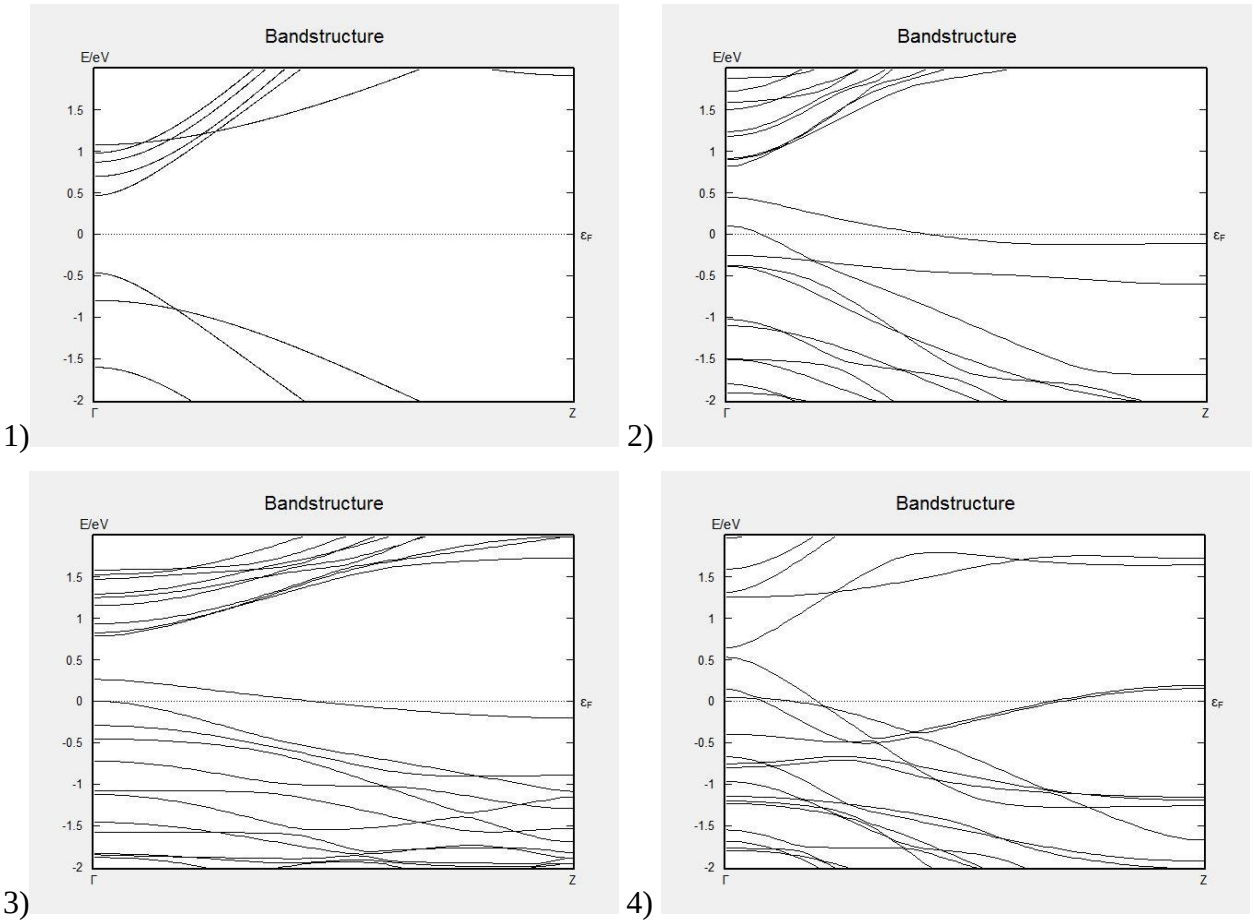

Figure 6-3 Band structure of pristine and Al-doped CNT (10, 0): 1) C_{40}, 2) $C_{39}Al$, 3) $C_{79}Al$, 4) $C_{38}Al_2$.

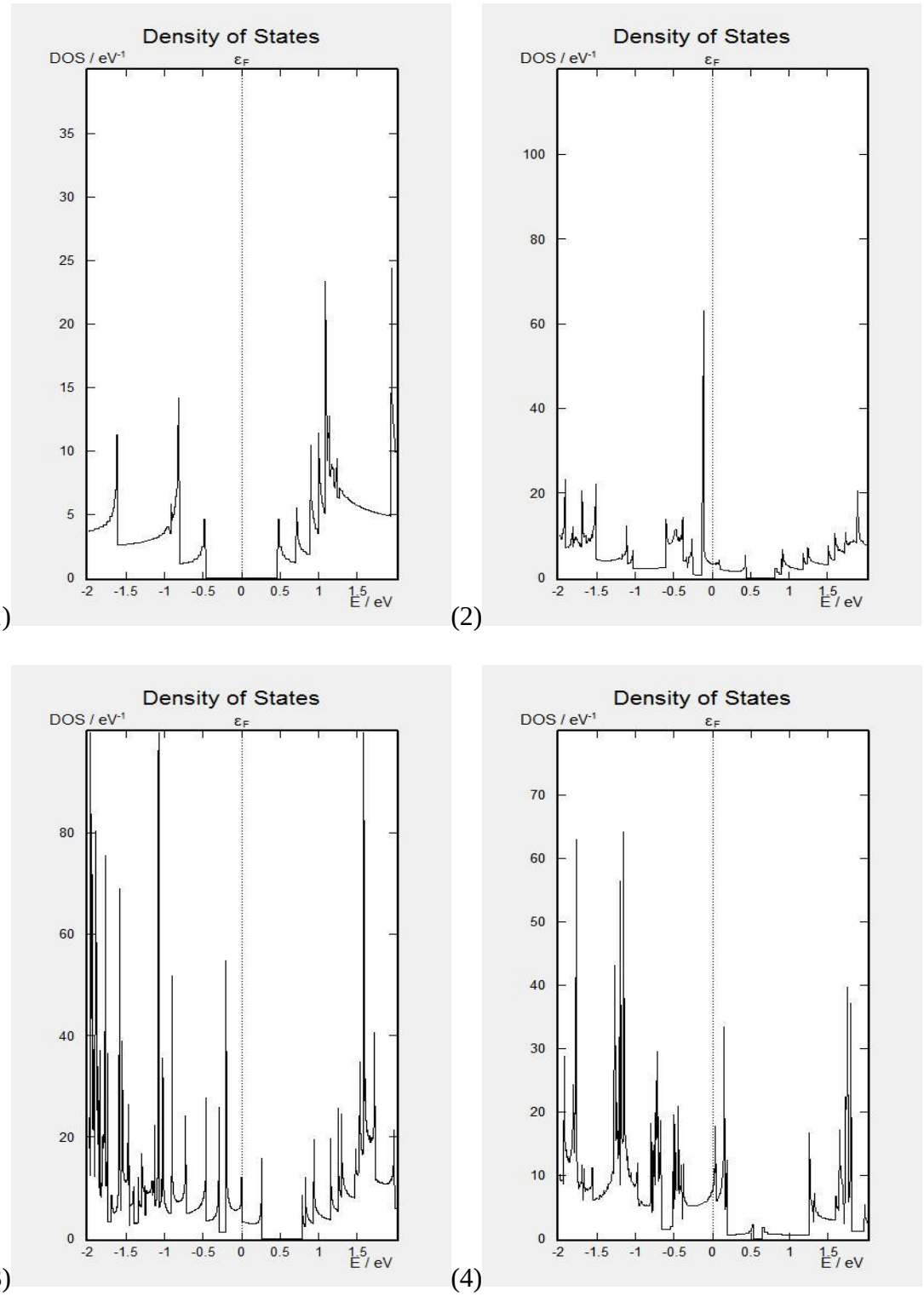

Figure 6-4 Density of states of pristine and Al-doped CNT (10, 0): 1) C_{40}, 2) $C_{39}Al$, 3) $C_{79}Al$, 4) $C_{38}Al_2$.

Table 6-1 Electronic structure of an Al-doped SWCNT (10, 0).

	Valence band maximum (eV)	Gap (eV)
C_{40}	-0.458	0.896
$C_{39}Al$	0.460	0.354
$C_{79}Al$	0.270	0.517
$C_{38}Al_2$	0.526	0.109

6.3.3 Copper doped SWCNT

To explore the potential of other metal doped SWCNT, Cu-doped SWCNT (10, 0) was also calculated to compare with the Al-doped SWCNT. It is found that Cu-doped SWCNT (10, 0) has a formation energy of 6.309eV which is larger than that of Al doped SWCNT in the same way as mentioned in the previous part of this report. It indicates the fact that Al-doped SWCNT is more energy favorable due to the stronger chemical bonding between Al-C than Cu-C. And with a doping rate 5% ($C_{38}Cu_2$), the valence band lift in the band structure which is similar as that in Al-doped SWCNT.

6.4 Conclusion

The study on the effects of Aluminum doping in the SWCNT was performed by using DFT calculation. From the result of geometry optimization and the total energy, it was discovered that the formation energy of doping Aluminum in a SWCNT is diameter and helicity dependent. From the result of the doping rate dependence on band structure and the density of states, the valence band lifting is observed in all the cases. At a low doping rate ($C_{39}Al$, $C_{79}Al$), localized band from Al dopants across the Fermi level indicates the semiconducting nature of the doped tube (10, 0). At a higher doping rate ($C_{38}Al_2$), the doped tube (10, 0) may transform to conducting which can be observed from the mixture of bands across the Femi level. And it is more challenging to dope Cu in SWCNT since it consumes more energy than Al does, though Cu doped SWCNT (10, 0) results in the similar band lift.

CHAPTER 7 : CONCLUSION

Nanoelectronics including copper based nanoscale interconnects have been experiencing significantly increased resistance that causes reduced calculation speed. Carbon nanotubes (CNTs) have been regarded as better interconnects due to its greater charge current carrying capability. However, the resistance of CNTs is not significantly better than that of copper based interconnects. This work was carried out to investigate to understand if and how metal (Cu, Al) with CNTs in the form of doping and hybrid metal/CNT nanowires can significantly increase the electric conduction of CNTs. Results have shown that encapsulation of Cu and Adsorption of Al atoms onto CNTs can introduce more states around Fermi level and thus the conductivity of nanowires is significantly increased that is greater than that of Cu nanowire with the same diameter. Adsorption of Al and substitutional doping of Cu or Al on CNTs can change semiconducting CNT to conducting, so that it skipped the selection and separation process from the received CNTs, since the synthesized CNTs is a mixture of metallic and semiconducting. Moreover, the end-contact of Al doped CNT with Al electrode was proved to show a smaller contact resistance which makes it a competitive candidate in practical applications in nanoelectronics such as interconnects.

REFERENCES

[1] S. Haykin, IEEE journal on selected areas in communications, 23 (2005) 201-220.

[2] S. Iijima, T. Ichihashi, (1993).

[3] Z. Ren, Z. Huang, J. Xu, J. Wang, P. Bush, M. Siegal, P. Provencio, Science, 282 (1998) 1105-1107.

[4] R. Schlittler, J.W. Seo, J. Gimzewski, C. Durkan, M. Saifullah, M. Welland, Science, 292 (2001) 1136-1139.

[5] A. Bachtold, P. Hadley, T. Nakanishi, C. Dekker, Science, 294 (2001) 1317-1320.

[6] A. Kongkanand, R. Martínez Domínguez, P.V. Kamat, Nano letters, 7 (2007) 676-680.

[7] A. Jones, T. Bekkedahl, C. Kiang, Nature, 386 (1997) 377.

[8] J. Li, Q. Ye, A. Cassell, H.T. Ng, R. Stevens, J. Han, M. Meyyappan, Applied Physics Letters, 82 (2003) 2491-2493.

[9] R. Saito, M. Fujita, G. Dresselhaus, u.M. Dresselhaus, Applied physics letters, 60 (1992) 2204-2206.

[10] A. Dergan, University of Ljubljana, (2010) 2-6.

[11] J.-C. Charlier, X. Blase, S. Roche, Reviews of modern physics, 79 (2007) 677.

[12] E.D. Minot, Cornell University, 2004.

[13] C.L. Kane, E. Mele, Physical Review Letters, 78 (1997) 1932.

[14] A. Kleiner, S. Eggert, Physical Review B, 64 (2001) 113402.

[15] S. Datta, Electronic transport in mesoscopic systems, Cambridge university press, 1997.

[16] W. Koch, M.C. Holthausen, A chemist's guide to density functional theory, John Wiley & Sons, 2015.

[17] M. Paulsson, arXiv preprint cond-mat/0210519, (2002).

[18] A.T. Version.

[19] S. Datta, IEDm: international electron devices meeting, 2002, pp. 703-706.

[20] K. Stokbro, J. Taylor, M. Brandbyge, H. Guo, Ab-initio non-equilibrium Green's function formalism for calculating electron transport in molecular devices, Introducing Molecular Electronics, Springer, 2006, pp. 117-151.

[21] H. Dai, A. Javey, E. Pop, D. Mann, W. Kim, Y. Lu, Nano, 1 (2006) 1-13.

[22] P.L. McEuen, M.S. Fuhrer, H. Park, IEEE transactions on nanotechnology, 1 (2002) 78-85.

[23] A. Javey, J. Guo, Q. Wang, M. Lundstrom, H. Dai, nature, 424 (2003) 654-657.

[24] B. Aïssa, D. Therriault, R. Farahani, L. Lebel, M. El Khakani, Nanotechnology, 23 (2012) 115705.
[25] M. Shiraishi, S. Nakamura, T. Fukao, T. Takenobu, H. Kataura, Y. Iwasa, Applied Physics Letters, 87 (2005).
[26] B.J. Landi, R.P. Raffaelle, S.L. Castro, S.G. Bailey, Progress in photovoltaics: research and applications, 13 (2005) 165-172.
[27] A. Du Pasquier, H.E. Unalan, A. Kanwal, S. Miller, M. Chhowalla, Applied physics letters, 87 (2005) 203511.
[28] C. Liu, Y. Fan, M. Liu, H. Cong, H. Cheng, M.S. Dresselhaus, Science, 286 (1999) 1127-1129.
[29] H.-M. Cheng, Q.-H. Yang, C. Liu, Carbon, 39 (2001) 1447-1454.
[30] X. Chen, D. Akinwande, K.-J. Lee, G.F. Close, S. Yasuda, B.C. Paul, S. Fujita, J. Kong, H.-S.P. Wong, IEEE Transactions on Electron Devices, 57 (2010) 3137-3143.
[31] N. Srivastava, K. Banerjee, ICCAD-2005. IEEE/ACM International Conference on Computer-Aided Design, 2005., IEEE, 2005, pp. 383-390.
[32] E. Durgun, S. Dag, V. Bagci, O. Gülseren, T. Yildirim, S. Ciraci, Physical Review B, 67 (2003) 201401.
[33] C.-K. Yang, J. Zhao, J.P. Lu, Nano Letters, 4 (2004) 561-563.
[34] F. Gao, J. Qu, M. Yao, Applied Physics Letters, 97 (2010) 242112.
[35] H.J. Hwang, O.-K. Kwon, J.W. Kang, Solid State Communications, 129 (2004) 687-690.
[36] C. Yang, Q. Chen, International Journal of Smart and Nano Materials, 4 (2013) 143-149.
[37] W. Kohn, L.J. Sham, Physical review, 140 (1965) A1133.
[38] D.M. Ceperley, B. Alder, Physical Review Letters, 45 (1980) 566.
[39] J.P. Perdew, A. Zunger, Physical Review B, 23 (1981) 5048.
[40] B. Hoefflinger, Chips 2020: a guide to the future of nanoelectronics, Springer Science & Business Media, 2012.
[41] B. Wei, R. Vajtai, P. Ajayan, Applied Physics Letters, 79 (2001) 1172.
[42] C.T. White, T.N. Todorov, Nature, 393 (1998) 240-242.
[43] J.-P. Salvetat, G.A.D. Briggs, J.-M. Bonard, R.R. Bacsa, A.J. Kulik, T. Stöckli, N.A. Burnham, L. Forró, Physical review letters, 82 (1999) 944.

[44] M.-F. Yu, O. Lourie, M.J. Dyer, K. Moloni, T.F. Kelly, R.S. Ruoff, Science, 287 (2000) 637-640.
[45] T.W. Tombler, C. Zhou, L. Alexseyev, J. Kong, H. Dai, L. Liu, C. Jayanthi, M. Tang, S.-Y. Wu, Nature, 405 (2000) 769-772.
[46] C.-K. Yang, J. Zhao, J.P. Lu, Physical Review B, 66 (2002) 041403.
[47] J. Jiang, C. Yang, Q. Chen, JOM, 68 (2016) 311-317.
[48] H. Yorikawa, S. Muramatsu, Physical Review B, 52 (1995) 2723.
[49] V. Bezugly, H. Eckert, J. Kunstmann, F. Kemmerich, H. Meskine, G. Cuniberti, Physical Review B, 87 (2013) 245409.
[50] Z. Jian-Min, D. Xiu-Juan, W. Su-Fang, X. Ke-Wei, Chinese Physics B, 18 (2009) 5468.
[51] Y. Matsuda, W.-Q. Deng, W.A. Goddard, The Journal of Physical Chemistry C, 111 (2007) 11113-11116.
[52] Y. Matsuda, W.-Q. Deng, W.A. Goddard Iii, The Journal of Physical Chemistry C, 112 (2008) 11042-11049.
[53] F. Gao, J. Qu, M. Yao, Applied Physics Letters, 96 (2010) 102108.
[54] N. Gao, J. Li, Q. Jiang, Applied Physics Letters, 103 (2013) 263108.
[55] C. Subramaniam, T. Yamada, K. Kobashi, A. Sekiguchi, D.N. Futaba, M. Yumura, K. Hata, Nature communications, 4 (2013).
[56] R.H. Baughman, A.A. Zakhidov, W.A. de Heer, science, 297 (2002) 787-792.
[57] S.J. Tans, A.R. Verschueren, C. Dekker, Nature, 393 (1998) 49-52.
[58] J. Guo, S. Datta, M. Lundstrom, IEEE transactions on electron devices, 51 (2004) 172-177.
[59] F. Gao, J. Qu, M. Yao, Journal of electronic packaging, 133 (2011) 020908.
[60] S. Dag, O. Gülseren, S. Ciraci, T. Yildirim, Applied Physics Letters, 83 (2003) 3180-3182.
[61] T. Meng, C.-Y. Wang, S.-Y. Wang, Journal of applied physics, 102 (2007) 013709.
[62] N. Park, S. Hong, Physical Review B, 72 (2005) 045408.
[63] A.N. Andriotis, M. Menon, Physical Review B, 76 (2007) 045412.
[64] A.N. Andriotis, M. Menon, Physical Review B, 78 (2008) 235415.
[65] Y. Matsuda, W.-Q. Deng, W.A. Goddard III, The Journal of Physical Chemistry C, 114 (2010) 17845-17850.
[66] Y. Kawakami, Y. Nojima, K. Doi, K. Nakamura, A. Tachibana, Electrochimica acta, 50 (2004) 739-744.

[67] N. Kulshrestha, A. Misra, D. Misra, Nanotechnology, 24 (2013) 185201.
[68] Q. Li, S. Fan, W. Han, C. Sun, W. Liang, JAPANESE JOURNAL OF APPLIED PHYSICS PART 2 LETTERS, 36 (1997) L501-L503.
[69] J.P. Perdew, K. Burke, M. Ernzerhof, Physical review letters, 77 (1996) 3865.
[70] A. QuantumWise, ReferenceManual/index. html.
[71] W.V. Glassey, R. Hoffmann, The Journal of Chemical Physics, 113 (2000) 1698-1704.
[72] C. Yam, Y. Mo, F. Wang, X. Li, G. Chen, X. Zheng, Y. Matsuda, J. Tahir-Kheli, W.A. Goddard Iii, Nanotechnology, 19 (2008) 495203.
[73] S.S. Yu, W.T. Zheng, Q. Jiang, IEEE Transactions on Nanotechnology, 9 (2010) 78-81.
[74] K. Jiang, L.S. Schadler, R.W. Siegel, X. Zhang, H. Zhang, M. Terrones, Journal of Materials Chemistry, 14 (2004) 37-39.
[75] S. Yang, G.-L. Zhao, E. Khosravi, The Journal of Physical Chemistry C, 114 (2010) 3371-3375.
[76] K. Gong, F. Du, Z. Xia, M. Durstock, L. Dai, science, 323 (2009) 760-764.
[77] R. Czerw, M. Terrones, J.-C. Charlier, X. Blase, B. Foley, R. Kamalakaran, N. Grobert, H. Terrones, D. Tekleab, P. Ajayan, Nano Letters, 1 (2001) 457-460.
[78] R. Wang, D. Zhang, W. Sun, Z. Han, C. Liu, Journal of Molecular Structure: THEOCHEM, 806 (2007) 93-97.
[79] J. Lu, X. Zhang, X. Wu, Z. Dai, J. Zhang, Sensors, 15 (2015) 13522-13532.
[80] R. Lee, H. Kim, J. Fischer, A. Thess, R.E. Smalley, Nature, 388 (1997) 255-257.
[81] Y. Zhao, J. Wei, R. Vajtai, P.M. Ajayan, E.V. Barrera, Scientific reports, 1 (2011).
[82] K. Choi, C. Yu, PloS one, 7 (2012) e44977.
[83] S.B. Yang, B.-S. Kong, D.-W. Kim, Y.-K. Baek, H.-T. Jung, The Journal of Physical Chemistry C, 114 (2010) 9296-9300.
[84] A.M. Rao, P. Eklund, S. Bandow, A. Thess, R.E. Smalley, Nature, 388 (1997) 257-259.
[85] J. Dai, J. Yuan, P. Giannozzi, Applied Physics Letters, 95 (2009) 232105.
[86] J. Yun, Z. Zhang, J. Yan, W. Zhao, M. Xu, Computational Materials Science, 108 (2015) 147-152.
[87] M. Jafari, M. Asadpour, N.A. Majelan, M. Faghihnasiri, Computational Materials Science, 82 (2014) 391-398.
[88] N.A. Lanzillo, N. Kharche, S.K. Nayak, Scientific reports, 4 (2014) 3609.